GRAIN BOUNDARY GROOVING OF PURE IRON IN NITROGEN SATURATED LIQUID LITHIUM

by

Lytle Briggs Whitefield III

ProQuest LLC.
789 East Eisenhower Parkway
P.O. Box 1346
Ann Arbor, MI 48106 – 1346

T-1727

SUBMITTAL SHEET

A Thesis submitted to the Faculty and the Board of Trustees of the Colorado School of Mines in partial fulfillment of the requirements for the degree of Masters of Science, Metallurgical Engincering.

Signed: Burkhead III
Student

Golden, Colorado

Date: Jan 9, 1975

Approved: David LeRoy Olson
Thesis Advisor

William M. Mueller
Head of Department

Golden, Colorado

Date: Jan 9, 1975

ABSTRACT

The mass transport behavior associated with an iron-liquid lithium interface was determined by a grain boundary grooving investigation. The controlling mass transport mechanism and the activation energy were determined for pure iron in a nitrogen saturated liquid lithium system.

The controlling mechanism was found by deduction of possible diffusion paths to be volume diffusion through the (Li-Fe-N) corrosion product on the surface of the alpha-iron. The mass transport of the iron was found to be coupled to and controlled by the diffusion of lithium through this corrosion product film.

The solid-liquid interfacial tension was determined and had a value of 2300 ergs/cm^2.

TABLE OF CONTENTS

LIST OF FIGURES

LIST OF TABLES

ACKNOWLEDGEMENTS

A graduate student seeks two major qualities in his thesis advisor: insight into the field, enabling the advisor to suggest a significant and challenging problem, and wisdom enabling him to guide the work to a meaningful problem. In this regard the author was fortunate, as he found these qualities in the man whom he worked for, Dr. David L. Olson. Dr. Olson's encouragement, suggestions, and guidance through all phases of the experimental program and analysis of the results were of great help.

The author gratefully appreciates the guidance and advice provided by the thesis committee, Dr. W. L. Bradley and Dr. D. K. Matlock. Appreciation is also expressed to Mr. Don Marts of Dow Chemical USA for his assistance in the preparation of the specimens.

Special thanks go to his wife, Anne, who has assumed the roles of mother and homemaker and for her financial support, understanding, encouragement and assistance.

This work was supported by the United States Atomic Energy Commission.

INTRODUCTION

Liquid alkali metals [1,2] are of primary interest as heat transfer fluids in advanced nuclear reactors and will also have a major role as electrodes in future high energy storage batteries. Alkali metals are so desired because of their large liquid temperature ranges with low melting temperatures, high thermal conductivities, low densities, and relative positions on the electromotive series.

The corrosion of the containment materials has unfortunately limited the use of these alkali metals. Liquid lithium, which is being considered as an energy transfer media for controlled thermonuclear reactors, is very corrosive to nearly all commerical structural alloys and ceramics. Alloys based on Nb and Ta and special carbide ceramics have shown [3,4,5] some capability of containing liquid lithium, but their use for large power reactors is economically restrictive. A number of ferrous alloys are being investigated [6-11] even though corrosion is occurring. The attempt is to determine the corrosion mechanism for these ferrous alloys and then hinder these atomic processes to achieve a corrosion rate acceptable to engineering design and expectations.

The liquid lithium corrosion behavior of pure iron, which does have a low corrosion rate compared to other ferrous alloys, is of interest since iron is the major component of all the ferrous alloys and must be understood if the corrosion behavior of multi-component

alloys is to be controlled.

Weight loss and penetration kinetics of iron and ferrous alloys in liquid lithium have been found[12,13] to have parabolic time dependency. This suggests that there is a mass transport controlling mechanism.

Capillarity,[20,21,22] the interfacial morphology governed by the minimization of interfacial free energy, was the driving force that was used in this investigation to determine the nature of the mass transport phenomena occurring at the interface of two condensed phases. Herring[23] related the interfacial tension to the chemical potential of an atom at this interface. Herring has shown that the chemical potential on a curved interface is given by the expression (in two dimensions x & y)

$$\mu = \mu_0 + \Omega\left(\gamma_{sl} + \frac{\partial^2 \gamma_{sl}}{\partial n_x^2}\right)K \qquad (1)$$

where

μ = chemical potential of an atom on a curved interface

μ_0 = chemical potential of an atom on a flat interface

K = curvature of the interface

γ_{sl} = interfacial tension

n_x = component of a unit normal to the interface

Ω = atomic volume

Equation 1 is a special form of the Gibbs-Thomson equation and an outline of the derivation of this expression is found in Appendix I. This expression, which relates chemical potential to interfacial tension

and curvature, suggests that for a general shaped interface, as is illustrated in figure 1, that there will be gradients in the chemical potential of atoms at this interface and thus a driving force for mass transport. The interfacial tension, γ_{sl}, is also a function of temperature, interfacial composition, and crystalline orientation.[25-27] The interfacial tension is given as a function of temperature from the thermodynamic relationship

$$\frac{\partial \gamma_{sl}}{\partial T} = -S \tag{2}$$

where interfacial entropy, S, is positive and indicates that the interfacial tension decreases with increasing temperature. The interfacial tension is given as a function of composition by the Gibbs Isotherm expression

$$\frac{\partial \gamma_{sl}}{\partial \mu_i} = -\Gamma_i \tag{3}$$

where Γ_i is the interfacial excess quantity of the component i and is defined to be

$$\Gamma_i = \frac{dN_i}{dA} \tag{4}$$

where N_i is the number of interfacial atoms of type i and A is the interfacial area. For a pure metal the excess quantity is zero, and thus, the interfacial specific free energy, f_s, is equal to the interfacial tension, γ_{sl}, as seen in the following relationship

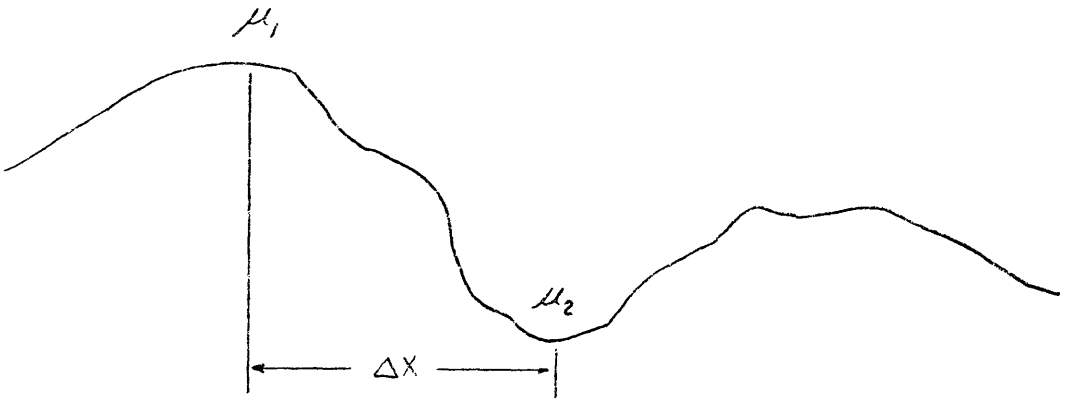

Figure 1. An interface with a general morphology. The driving force for mass transport of these atoms at the interface is given by $-\frac{\Delta \mu}{\Delta X}$.

$$f_s = \gamma_{sl} + \sum_{i=1}^{n} \mu_i \Gamma_i \qquad (5)$$

For this case involving a lithium-iron interface in which both components are very insoluble in each other, the condition that the interfacial free energy equals the interfacial tension will be assumed. It will be considered that if the interfacial tension changes as a function of composition (as seen from equation 3) it is due to a third component or a contaminate. It is possible for the lithium-iron system that carbon or nitrogen may influence the interfacial tension in this manner.

With the number of broken bonds depending on the orientation of the interface formed, it is expected that the work necessary to form this interface, and the associated interfacial tension, is also a function of orientation with respect to the crystalline lattice. This broken bond concept was used by Moore, Mackenzie, and Nichols[24] to calculate the interfacial energy for FCC metals as is seen in figure 2. A number of investigators[25,26,27] have measured this variation in interfacial tension as a function of orientation for pure gold, copper, and nickel.

The interfacial tension has been found to be a function of temperature, composition, and crystalline orientation and for this investigation an approximate value for the interfacial tension, γ_{sl}, will be determined.

The flux, J, can be given in its most general form:

$$J = cv \qquad (6)$$

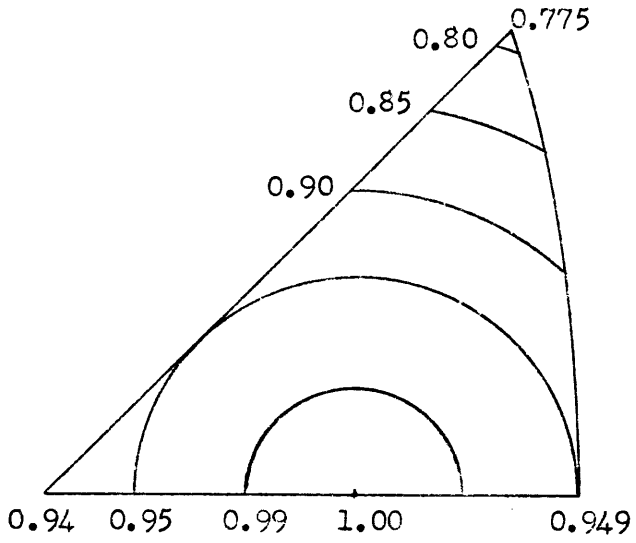

Figure 2. The theoretically determined γ-plot for FCC metals from the broken-bond model of Moore. The plot indicates the normalized surface tensions as a function of crystal orientation.

where c is the concentration of atoms moving and v is the velocity of these atoms. The velocity can be related to the driving force, F, by the following expression

$$v = MF \tag{7}$$

where M is the mobility. With the Nernst-Einstein relationship,[28] the mobility can be given as

$$M = D/kT \tag{8}$$

where D is the diffusion coefficient for the diffusing atoms and kT has the conventional meaning. Substituting equation 7 and 8 into equation 6, the flux can be related to the driving force by the following equation

$$J = \frac{cD}{kT} F \tag{9}$$

From mechanics the force can be related to the negative of the gradient of potential. Thus, for the case of varying chemical potential as a function of surface morphology (figure 1), the flux equation can be written as

$$J = -\frac{cD}{kT} \nabla\mu \tag{10}$$

Equation 1 and 10 express the desire for relaxation by mass transport of a perturbed interfacial morphology. The atom flux will continue until the chemical potential gradient vanishes.

Mullins[14,29-32] has determined the rate of morphological change

for simple geometries and found that all the linear dimension are proportional to some simple time dependent scale law. The following simple geometries where Mullins' work on rate of morphological change has been applied are:

a. Growth of grain boundary grooves

b. Growth of a facet

c. Relaxation of an infinite sinusoidal profile

d. Decay of isolated scratches

Mullins obtained mathematical expression for morphological changes by the various modes of possible mass transport mechanisms. For example, Mullins obtained the following differential equations for morphological changes as a function of y, x, and t due to the divergence of interfacial flux, the following general equation was derived

$$\frac{\partial y}{\partial t} = -B \frac{\partial^4 y}{\partial x^4} \tag{11}$$

with

$$B = \frac{D_s \gamma_{sl} \Omega^2 N}{kT} \tag{12}$$

where

D_s - interfacial diffusion coefficient

N - number of interfacial atoms per square cm

Mullins[32] has derived an exact solution for describing morphological changes associated with grain boundary grooving by interfacial diffusion. This analysis assumes that the grain boundary is perpendicular to the

interface, the diffusion coefficient is isotropic and the interfacial tension is constant. Figure 3 illustrates the grain boundary profile for Mullins' analysis. The solution to equation 11, for this case, when interfacial diffusion is the controlling process is given by the expression

$$y(x,t) = m(Bt)^{1/4}Z(u) \tag{13}$$

where

$$m = \gamma_{gb}/2\,\gamma_{sl}$$

γ_{gb} = grain boundary energy

$$u = x/(Bt)^{1/4}$$

Expanding Z(u) in a power series and plotting u as a function of Z(u), the width of the groove, w_s (relating the separation of the maxima), as a function of time due to interfacial diffusion is found to be

$$w_s = 4.6(Bt)^{1/4} \tag{14}$$

and similarly the depth of the groove, d_s, as a function of time due to interfacial diffusion is found to be

$$d_s = 0.973\ m(Bt)^{1/4} \tag{15}$$

Equations 14 and 15 relate the measureable linear dimensions, w_s and d_s, to the rate coefficient for the controlling process, which for this case is interfacial diffusion. The determination of such rate coefficients by experimental measurements of groove morphology is the basis of approach of this investigation to understand the mass transport behavior at, or near, the liquid lithium-iron interface.

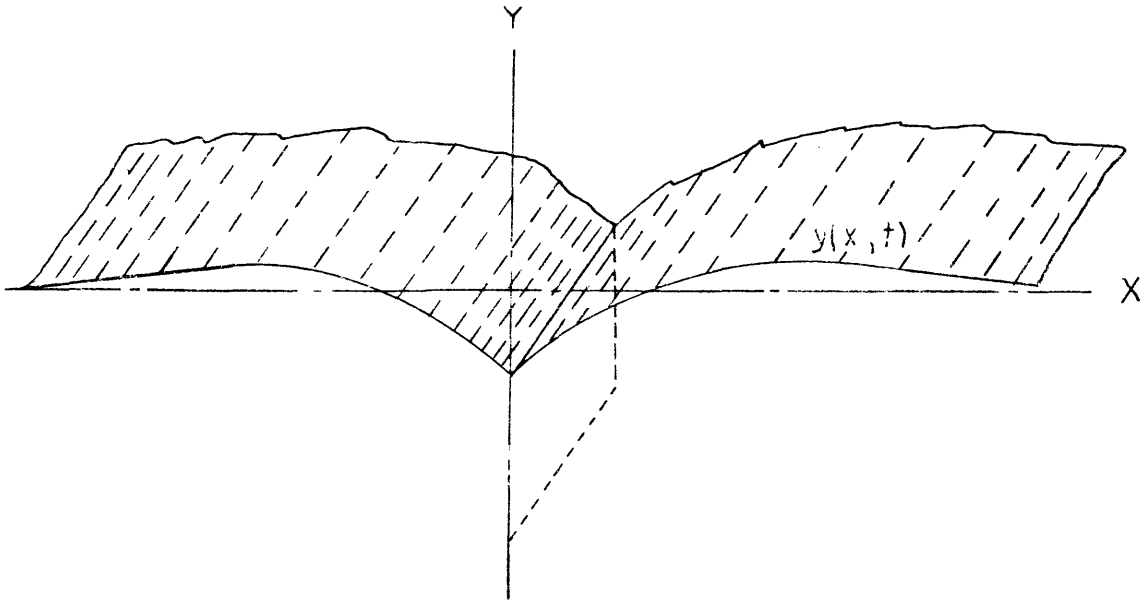

Figure 3. Profile of a thermal groove

For the case of volume diffusion through either the bulk or liquid phase Mullins[31] has determined the morphological changes as a function of y,x,t due to the divergence of volume diffusion flux for grain boundary grooving. The changes in groove width, w_v, and groove depth, d_v, for volume diffusion controlled grain boundary grooving has been found to be given by

$$w_v = 5.0\ (Ct)^{1/3} \tag{16}$$

where

$$C = \frac{C_o D_v \gamma_{sl} \Omega^2}{kT} \tag{17}$$

where

D_v = volume diffusion coefficient of diffusing atoms

C_o = concentration of diffusing atoms in the phase which the diffusion is occurring

and similarly, the depth of the groove, d_v, as a function of time due to interfacial diffusion is found to be

$$d_v = 1.01\ m(Ct)^{1/3} \tag{18}$$

This derivation by Mullins for volume diffusion controlled grooving is outlined in Appendix II.

A wealth of surface self diffusion data for metals[33-40] has been determined by measuring thermal grooving kinetics in vacuum, hydrogen or inert gases. A number of thermal grooving investigations have been performed for interfaces between condensed phases. Kruger

and Stern[41] have determined the grain boundary grooving kinetics on silver in molten NaCl. Steidel et al[42] have performed grain boundary grooving on Nickel in a saturated Ni-S liquid. Feingold et al[43] investigated the mass transport behavior associated with a solid nickel-Al_2O_3 interface by this thermal grooving method.

Eberhart et al[44] determined by grain boundary grooving of alpha-iron in liquid sodium the mass transport mechanism. They obtained log groove width versus log time plot (figure 4) which indicates interfacial diffusion control. Also the h/d ratio gave values again consistent with interfacial diffusion. Eberhart et al[44] calculated the interfacial diffusion coefficients and plotted them in an Arrhenius plot (figure 5) to determine an activation energy of 37 Kcal./Mole for this interfacial diffusion process.

The primary interest of this investigation is to determine the nature of the mass transport phenomena occurring at, or near, the liquid lithium-solid iron interface. This information is to be obtained be determining the kinetics for the relaxation of a perturbed interface by measuring the rate of grain boundary grooving[14] of Armco iron in nitrogen saturated liquid lithium at elevated temperatures. These experiments were designed to have stress free iron in contact with quiescent isothermal nitrogen saturated liquid lithium in a container of chemically identical material as the specimen. Therefore this investigation will not have interferences from thermal gradients,[15,16]

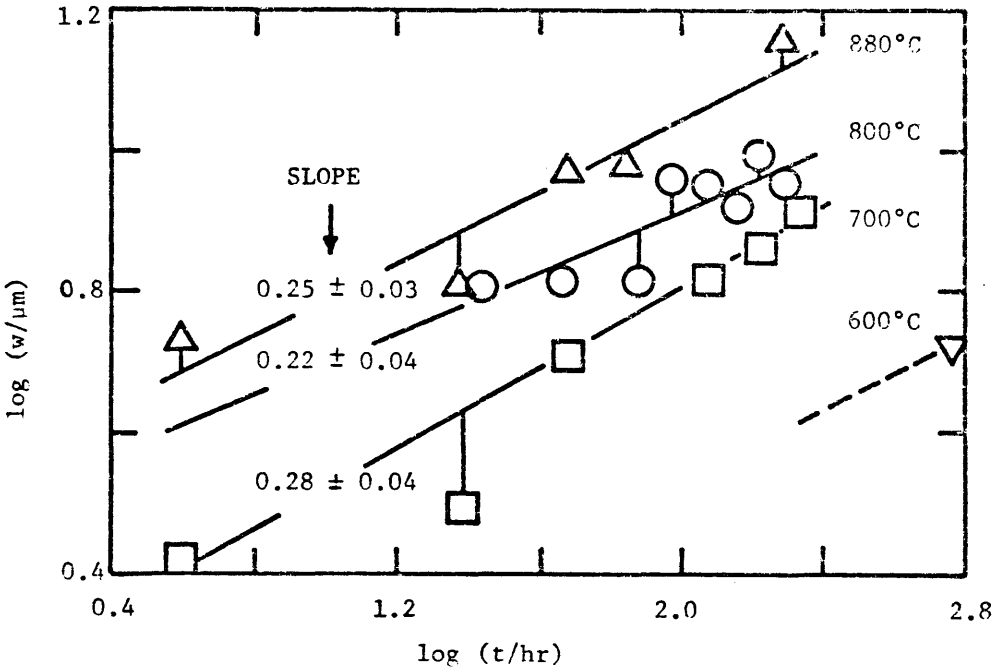

Figure 4. A plot of log groove width versus log time for grain boundary grooving of iron in liquid sodium.

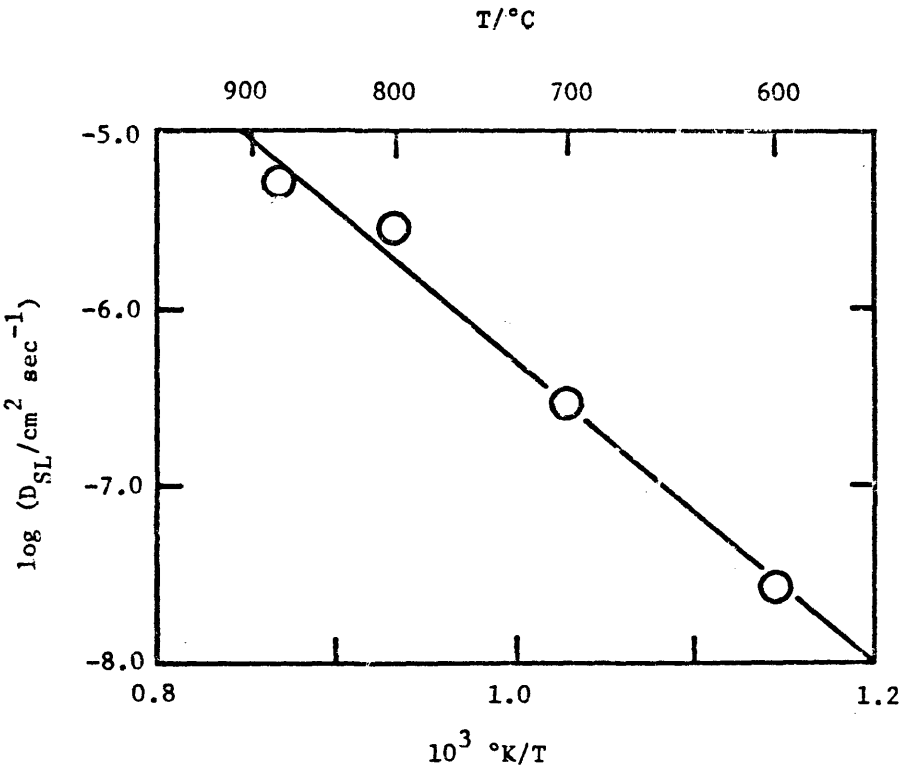

Figure 5. An Arrhenius plot for grain boundary grooving of iron in liquid sodium.

dissimilar metal mass transport[17,18] or stress corrosion cracking.[10,19]

EXPERIMENTAL PROCEDURE

Materials

High purity lithium, 99.9%, was used as the corrosive medium for this investigation. The lithium was purchased from the Research Organic Inorganic Chemical Corporation and was shipped submerged in mineral oil within a sealed stainless steel container. The received lithium was covered with a black lithium nitride scale.

Armco electrolytic iron was chosen as the material for the specimens. The composition of this material is illustrated in Table I. To ensure there were no dissimilar metal effects, all metal that came into contact with the lithium was Armco iron.

The Armco iron was received in two different sizes of rod. The material was chemically identical. The diameter of the large rod was 2.750 inches and the diameter of the small rod was 0.375 inches. The large diameter alpha-iron rod was used for the crucible and lid, and the small diameter rod was used for specimens. The alpha-iron grain size of the as received Armco iron was number 7 by ASTM standards. This grain size was too small for measurements by interference microscopy, which was used to measure the linear dimensions of the thermal groove. In order to grow the grains to sufficent size, the iron specimens were cold worked by 50 per cent reduction in a hydraulic press to guarantee recrystallization and growth by the subsequent heat treatment. The iron was annealed in a reducing atmosphere (N_2-15%H_2) at 895°C for 4 hours and allowed to furnace cool. The reducing atmosphere was used to

TABLE I

Maximum Impurity Composition (in wt. %) for the Armco Iron Specimens.

Element	Maximum Weight %
C	.01
Mn	.07
P	.008
S	.02
Si	.02
Al	.05
Ti	.03

minimize the formation of an oxide on the specimen. Following the heat treatment the specimen was cleaned of any possible oxide film on the surface by grinding. Once the specimen had been thoroughly cleaned of surface contaminates it was polished by mechanical means using 1.0 micron diamond polish. By grinding and polishing the specimen flat the equilibrium condition for the grain boundary groove was perturbed.

All thermal grooving tests were conducted within a stainless steel glove box using pure argon gas (99.98%) as a cover gas. The glove box atmosphere was further purified by continually skimming the surface of a pool of eutectic sodium-potassium alloy. When the surface of this sodium-potassium alloy was free of an oxide film, it was assumed that the oxygen contamination level was extremely low.

The nitrogen level in the glove box atmosphere was controlled by lithium-nitrogen equilibrium. A lithium-nitride surface scale, indicating nitrogen saturation, was observed each time the test crucible was opened. This suggested the nitrogen concentration in the liquid lithium was at saturation.

APPARATUS

Figure 6 illustrates the test crucible and lid arrangement. The baffles were incorporated to minimize the loss of lithium vapors. The lithium vapors would rise and condense on the baffles and droplets would fall back into the liquid lithium. The liner and crucible were designed so that when a specimen was lowered into the crucible it would be

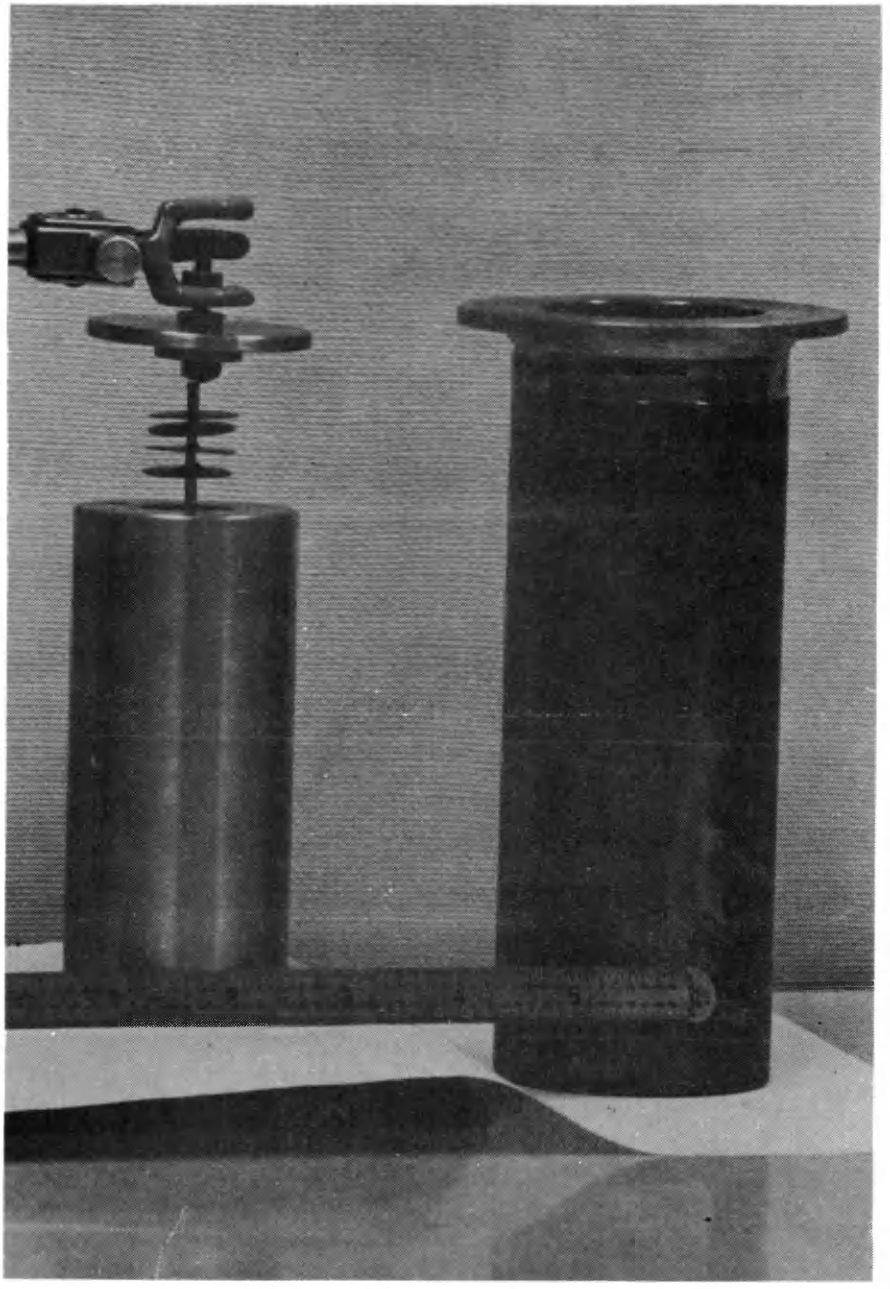

Figure 6. Pure Armco iron crucible and lid with baffle design. To the extreme right is the protective furnace liner.

located in the center of the hot zone; thus, temperature fluctuations were minimized. The liner also served as a failsafe device for the furnace coils in the event the crucible failed. The furnace was a Lindberg model 56312A and was controlled by a Marshall 4044 proportional controller which provided a temperature control of ± 2°C.

TESTING

The test was initiated by charging the crucible with lithium that had been wiped clean to remove surface contaminates and mineral oil. For each new temperature lithium was added to the crucible to bring the level of the liquid lithium up to the original height.

At the beginning of this corrosion investigation the furnace was heated to 800°C and pure iron filings were dropped into the liquid lithium charge. The temperature of 800°C was chosen for two reasons. The first reason was that at 815°C the Li_3N compound dissociates which in turn could effect the solubility of iron in lithium (figure 7). The second reason was that this was the maximum test temperature for this investigation. After a period of approximately 20 hours the furnace was turned off.

The addition of iron filings was made to ensure iron saturation of the lithium. In addition to this initial effort of ensuring iron saturation of the lithium, the furnace was turned on at least four hours prior to the start of any test, and thus, allowed the equilibrium conditions to be reached for that given test temperature. The specimen

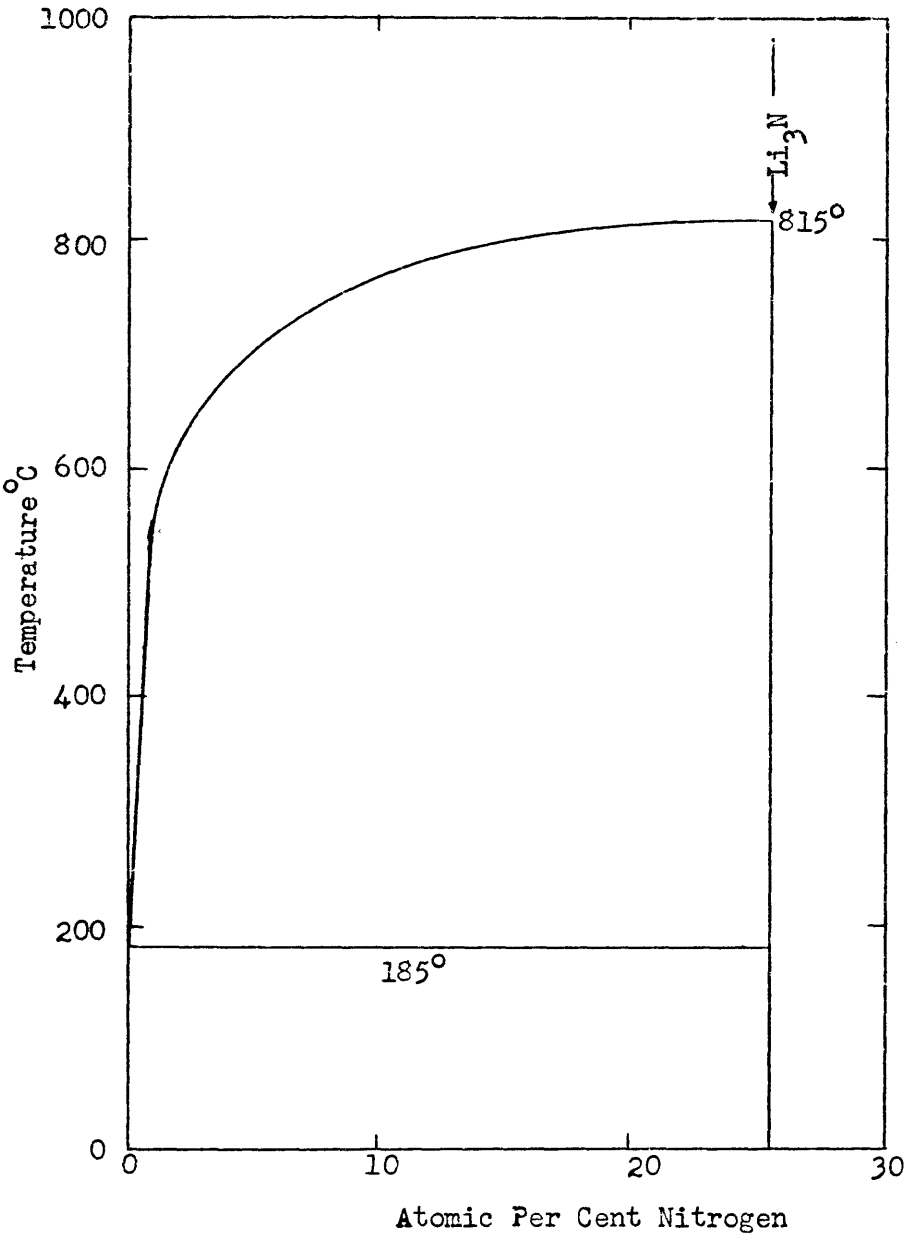

Figure 7. The Li_3N portion of the lithium-nitrogen equilibrium phase diagram.(54)

was then suspended in the central region of the liquid lithium for a predetermined period of time. To ensure the specimen was placed in the same region each time, the distance form the specimen to the baffle support was measured and maintained. At the end of this time interval, the specimen was removed from the lithium and placed on a large copper plate. This procedure was adopted to minimize and cool-down effects. The specimen was then cleaned of any lithium on the surface by submersion into water at room temperature and then examined. Following the initial time interval of each new test temperature certain grain boundaries were marked with a Tukon hardness tester so that after each successive interval of time the same grain boundary would be examined. The examination was conducted using Leitz microscopy with a Tolansky kual beam interferometer attachment. The grain boundaries of interest were photographed (figure 8) with a 35mm Leitz camera attached to the microscope.

In grain boundary grooving experiments two linear dimensions can be measured, the width of the groove and the depth of the groove. The width of the groove was chosen to be measured for this investigation. A two millimeter scale was photographed on each film strip in addition to the grain boundaries of interest. This procedure provided a convenient way to determine the magnification of the micrograms and was used also to measure the groove widths. The groove widths were measured from the maximas along the x-axis. The enlargement of the negatives was performed using a Griscombe microfilm reader,

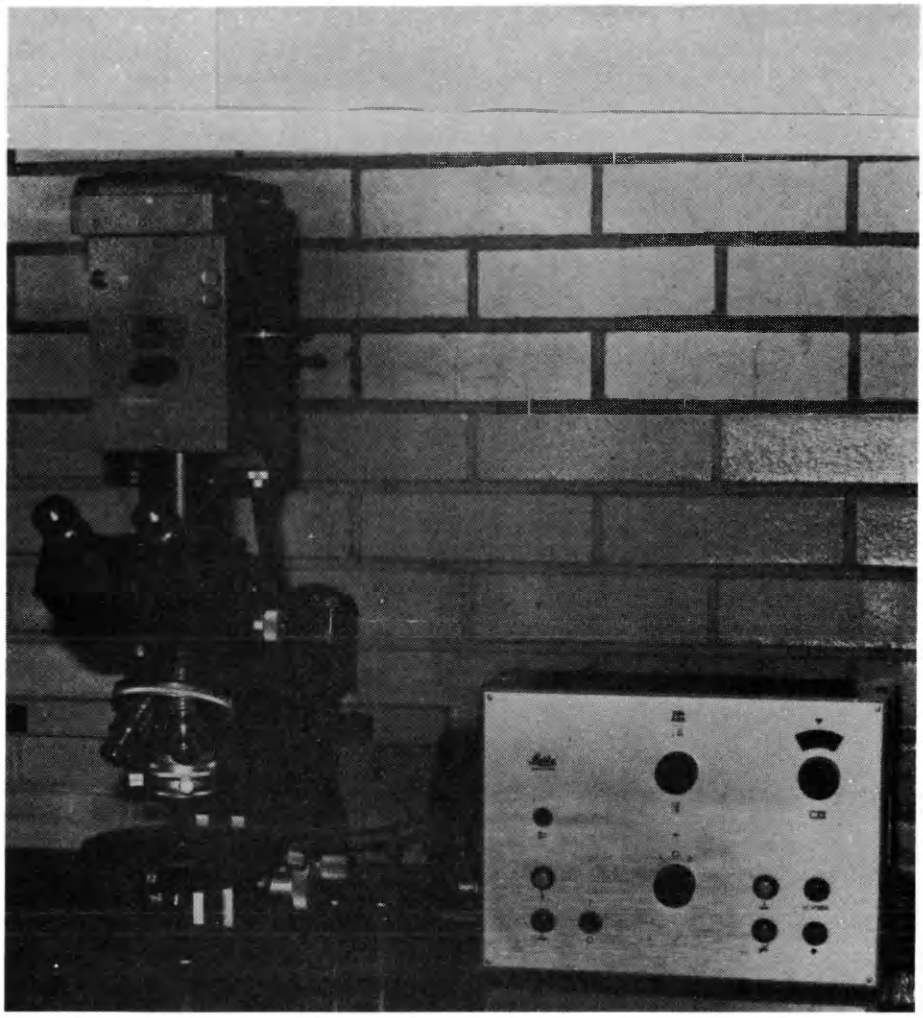

Figure 8. Leitz microscope with a Tolansky dual beam interferometer attachment.

model PA.

A typical interferogram of a flat surface and of a grain boundary groove is illustrated in figure 9. The observed fringes resulting from sodium light reconstruction corresponds to a fringe spacing of 2945 Å of surface relief. After the film was developed and the groove widths measured, the sample was suspended from the crucible lid and transferred into the glove box to again be submerged into the liquid lithium. After the last interval of time for each temperature, the groove angle was also measured.

Thermal grooving tests were conducted at 600°C, 650°C, 700°C, 750°C, and 800°C. The duration of the test for 600°C was 85 hours, and 19 hours for the 800°C test.

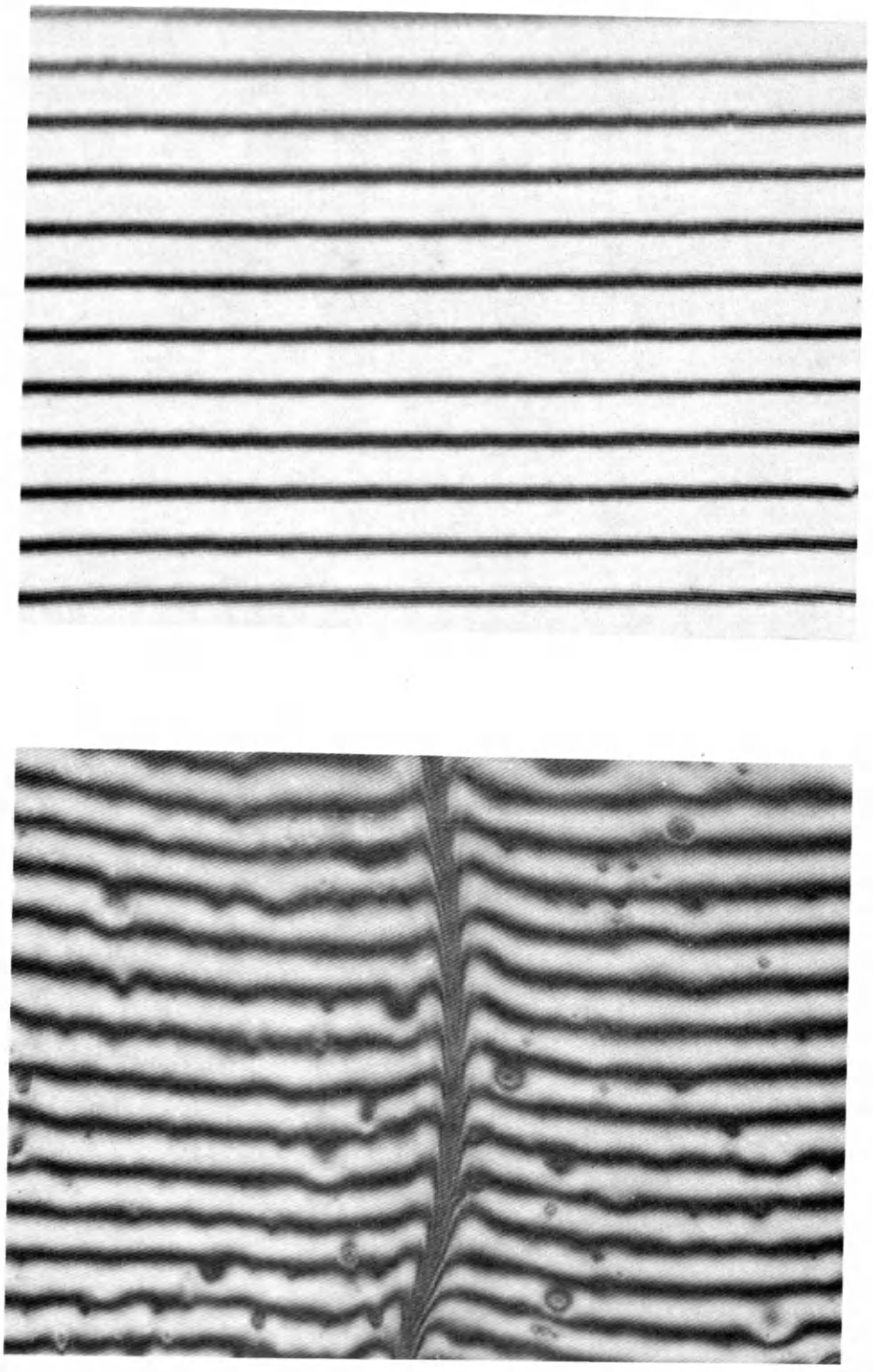

Figure 9. Interferograms of a flat surface (top) and of a grain boundary groove (bottom). The fringe spacing represents one-half wave length (2945 Å).

RESULTS AND DISCUSSION

Many studies of interfacial and volume self diffusion of metals have been performed in recent years[14,33-40,44] by measuring grooving kinetics in different environments. The purpose of this investigation was to determine the mass transport mechanism occurring at, or near, the liquid lithium-iron interface. In addition to determining the controlling mechanism for the process, the diffusion coefficients and an activation energy were found.

Once the width of the grain boundary groove was obtained, a plot of the log of the groove width versus log of time was constructed (figures 10-14). These plots were useful in the determination of the proper time dependency, and thus, the proper scale law. Figure 10, also illustrates the transient behavior before the grain boundary groove attained an equilibrium dihedral angle. The duration of this transient behavior was found to decrease as the temperature increased. This phenomena is expected to be the result of variation in grain boundary energy due to the lithium grain boundary penetration. From equation 16, it can be seen that for the case of volume diffusion as the controlling mechanism, the plot of log w_v versus log time, the slope will be 0.33. Table II shows the resulting slopes for the plots obtained for the 600°C, 650°C, 700°C, 750°C, and 800°C tests. Examination of this table suggests the controlling mechanism to be volume diffusion.

Another technique for determining the mechanism of grain boundary grooving was the examination of individual thermal groove profiles.

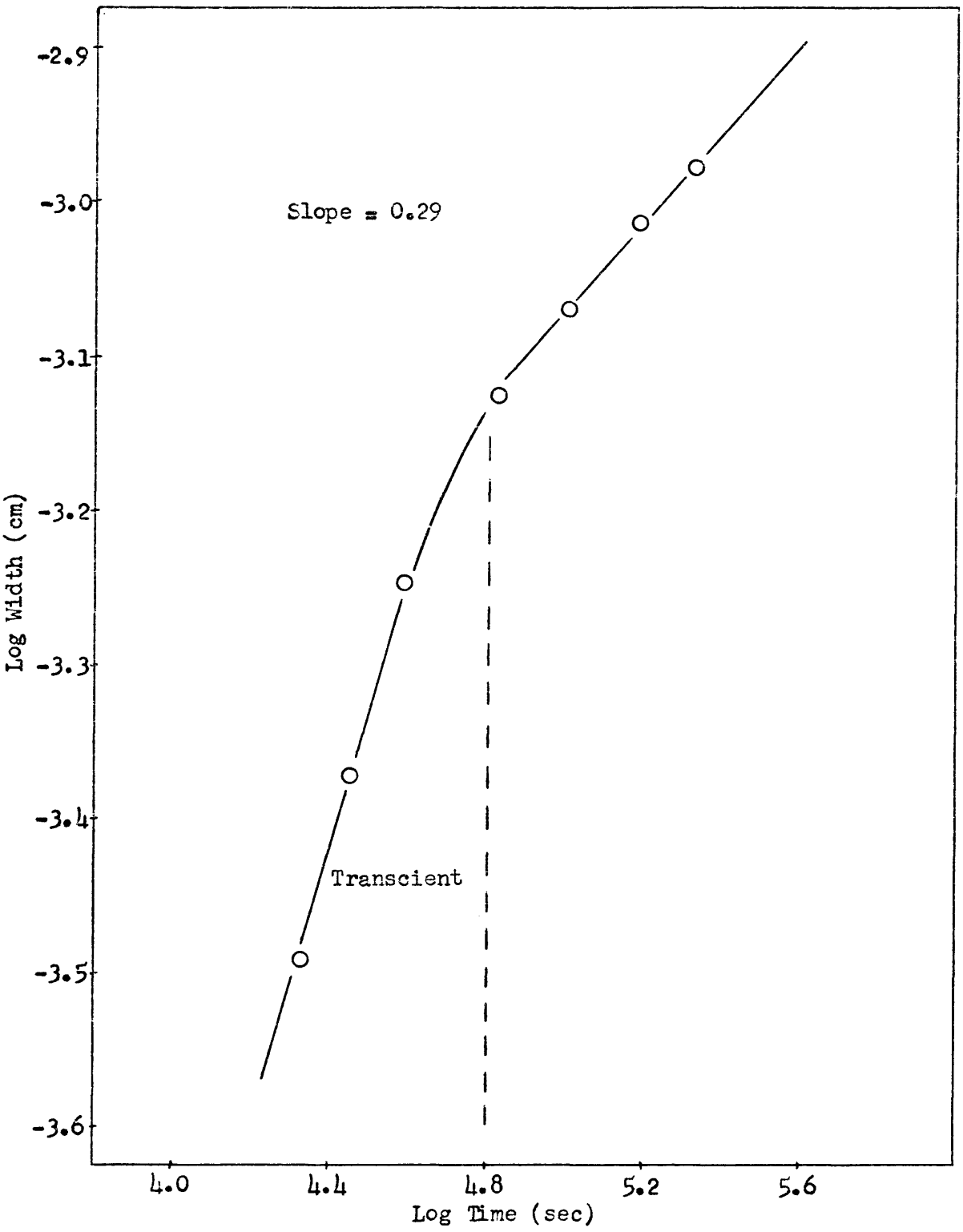

Figure 10. Graph of Log Groove Width vs. Log Time for pure iron in liquid lithium at 600 C.

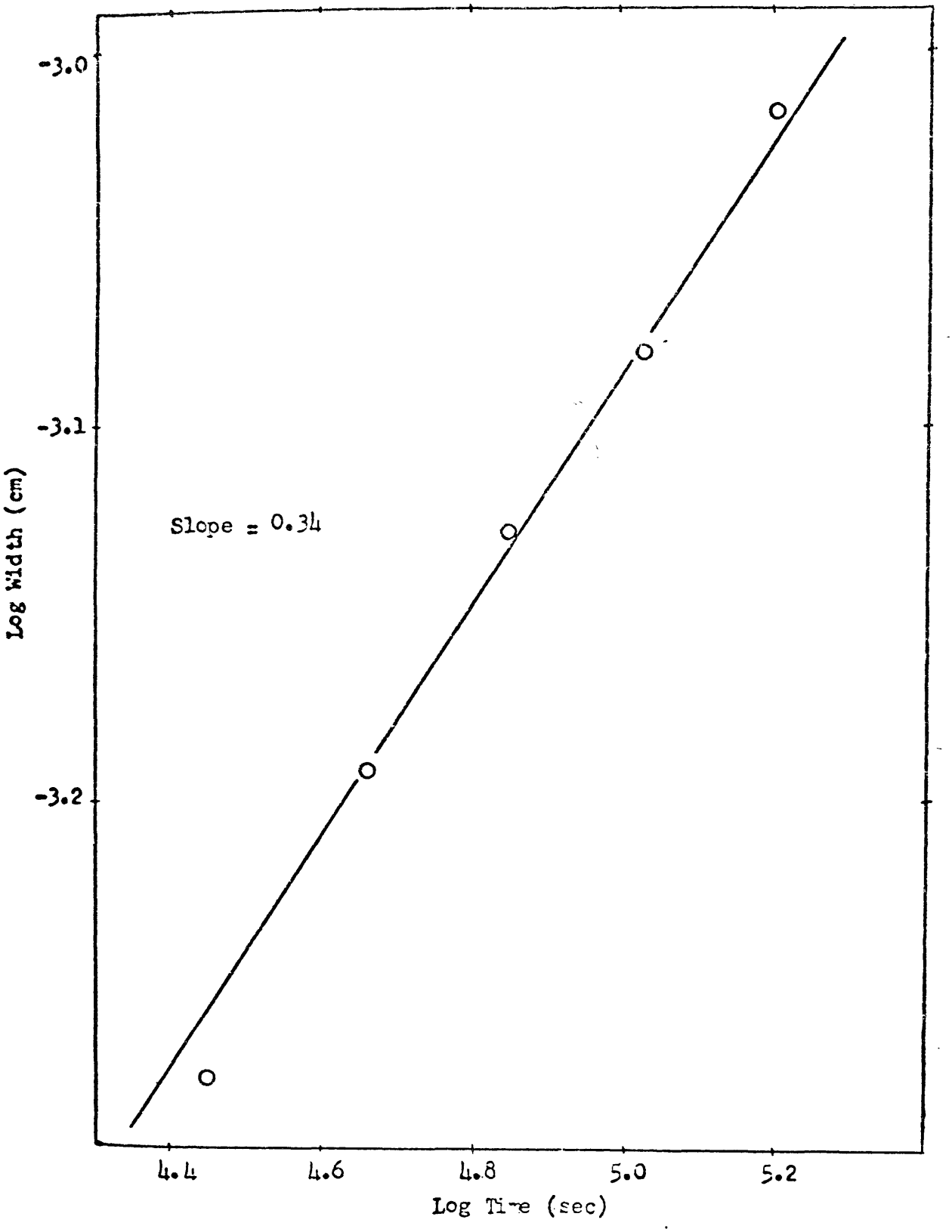

Figure 11. Graph of Log Groove Width vs. Log Time for pure iron in liquid lithium at 650 C.

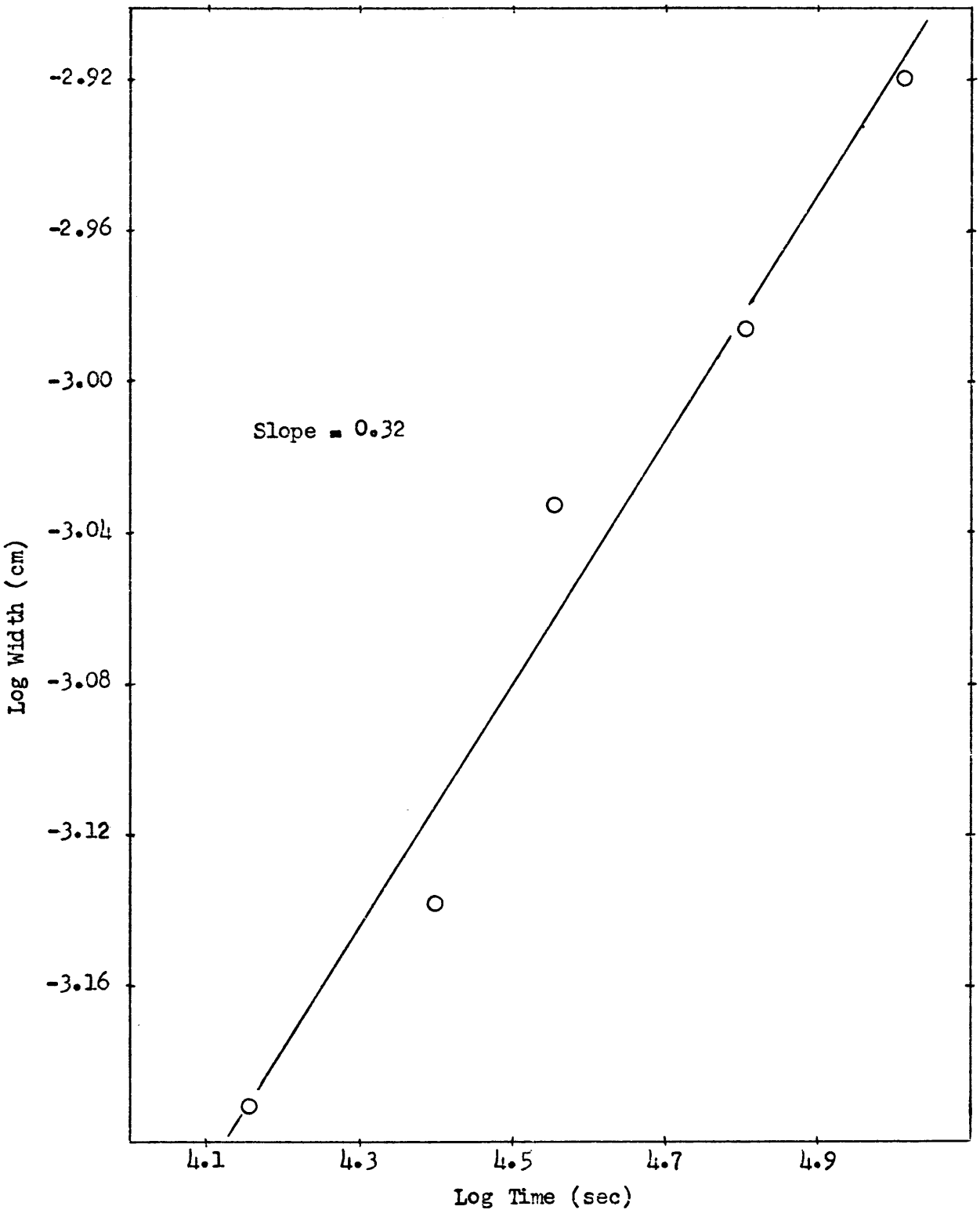

Figure 12. Graph of Log Groove Width vs. Log Time for pure iron in liquid lithium at 700 C.

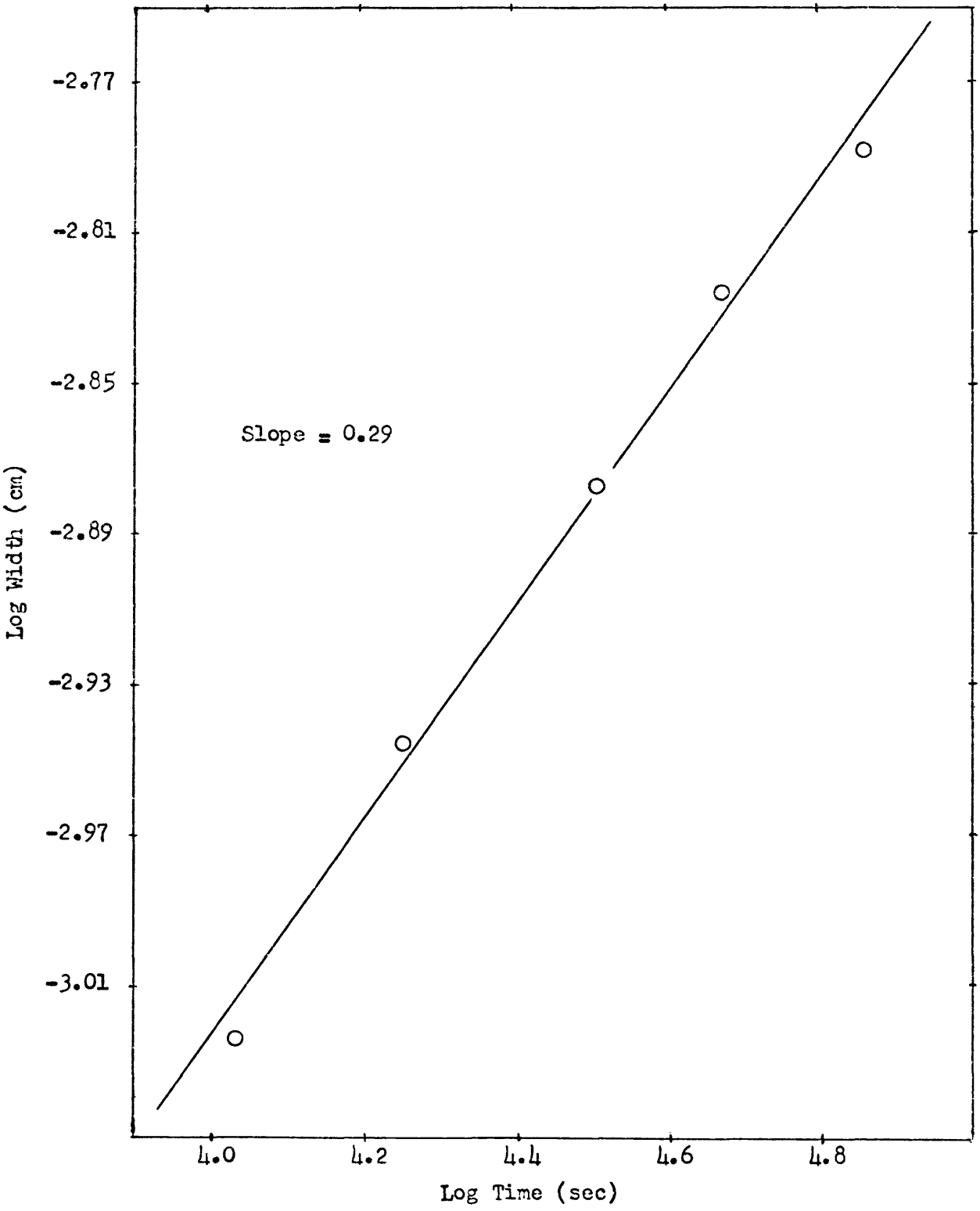

Figure 13. Graph of Log Groove Width vs. Log Time for pure iron in liquid lithium at 730 C.

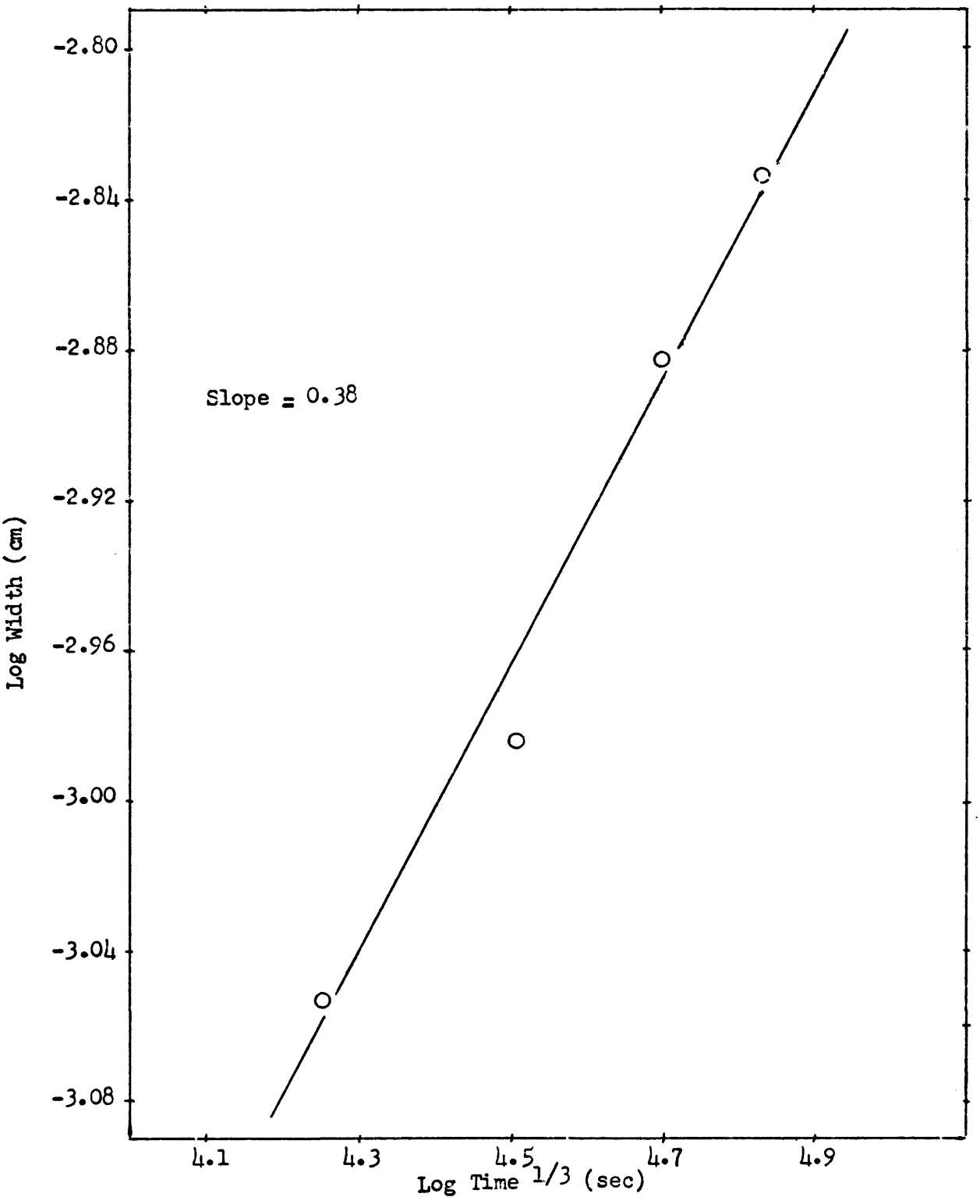

Figure 14. Graph Log Groove Width vs. Log Time for pure iron in liquid lithium at 800 C.

TABLE II

Resulting Slopes for plots of Log Width versus Log Time

Temperature, ^{o}K	Slopes
873	0.29
923	0.34
973	0.32
1023	0.29
1073	0.38
Mean value of slopes:	0.32

Mullins' theory[14,31] found the profile of a grain boundary groove formed by interfacial diffusion different from one formed by volume diffusion. Allen[45] has investigated this difference and found that the ratio of ridge height of the groove, h, to the ridge depth of the groove, d, given by

$$h/d = 0.208 \quad \text{for interfacial diffusion} \tag{19}$$

and

$$h/d = 0.149 \quad \text{for volume diffusion} \tag{20}$$

Both h and d were measured for a number of groove profiles and the results obtained had a mean ratio of 0.143, which also indicated the controlling process was volume diffusion.

In order to determine the diffusion coefficients and an activation energy for the controlling process the expression for the rate coefficients must be defined. For the case of volume diffusion as expressed by equation 16, the measured rate coefficient, K, for time$^{1/3}$ dependence, would be given by

$$K = 5.0\, C^{1/3} \tag{21}$$

The rate coefficients for the various temperatures can be obtained as the slope of the plots of width verses time$^{1/3}$ (figures 15-19). These results are tabulated in Table III for the corresponding temperatures.

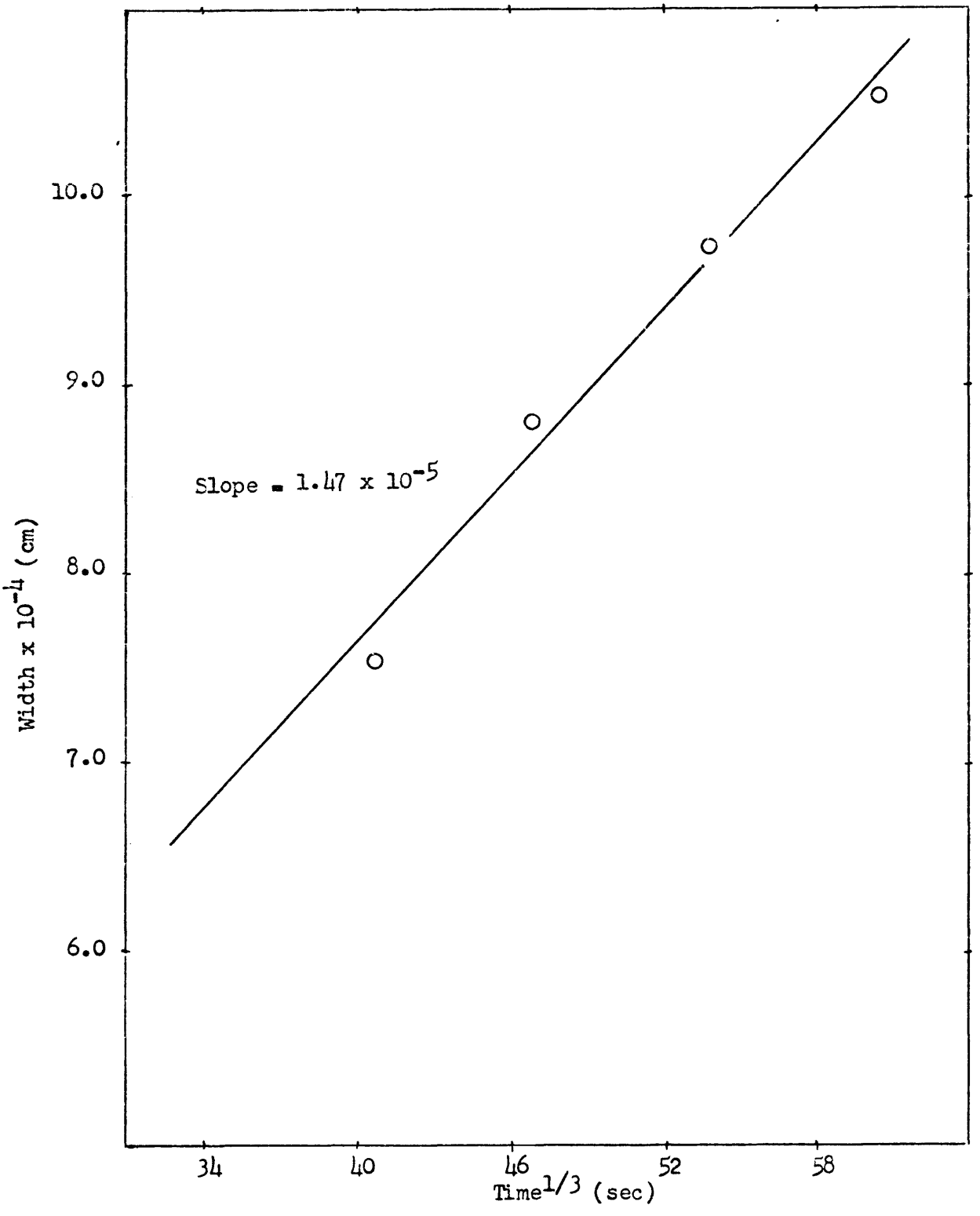

Figure 15. Graph of Groove Width vs. Time$^{1/3}$ for pure iron in liquid lithium at 600 C.

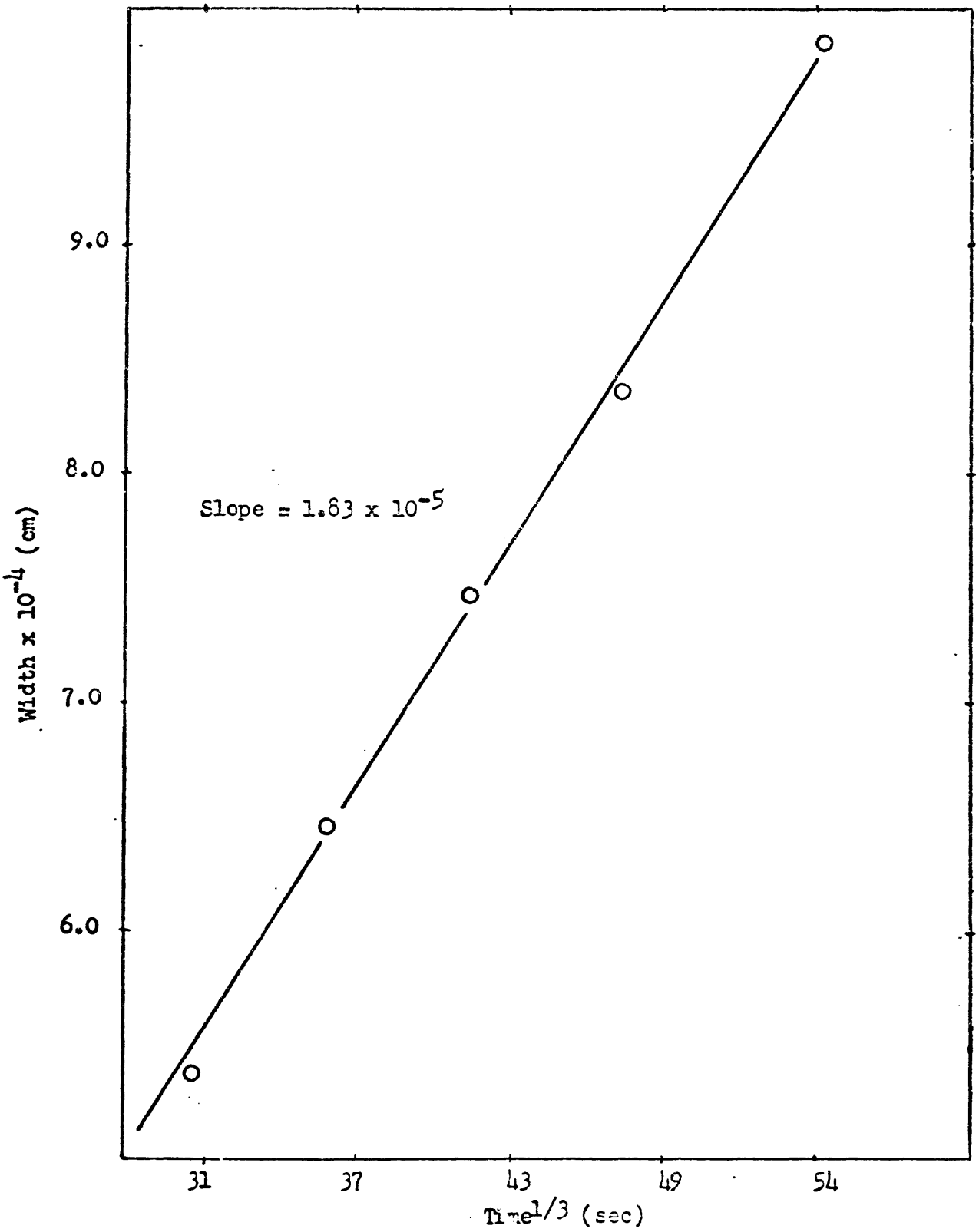

Figure 16. Graph of Groove Width vs. $Time^{1/3}$ for pure iron in liquid lithium at 650 C.

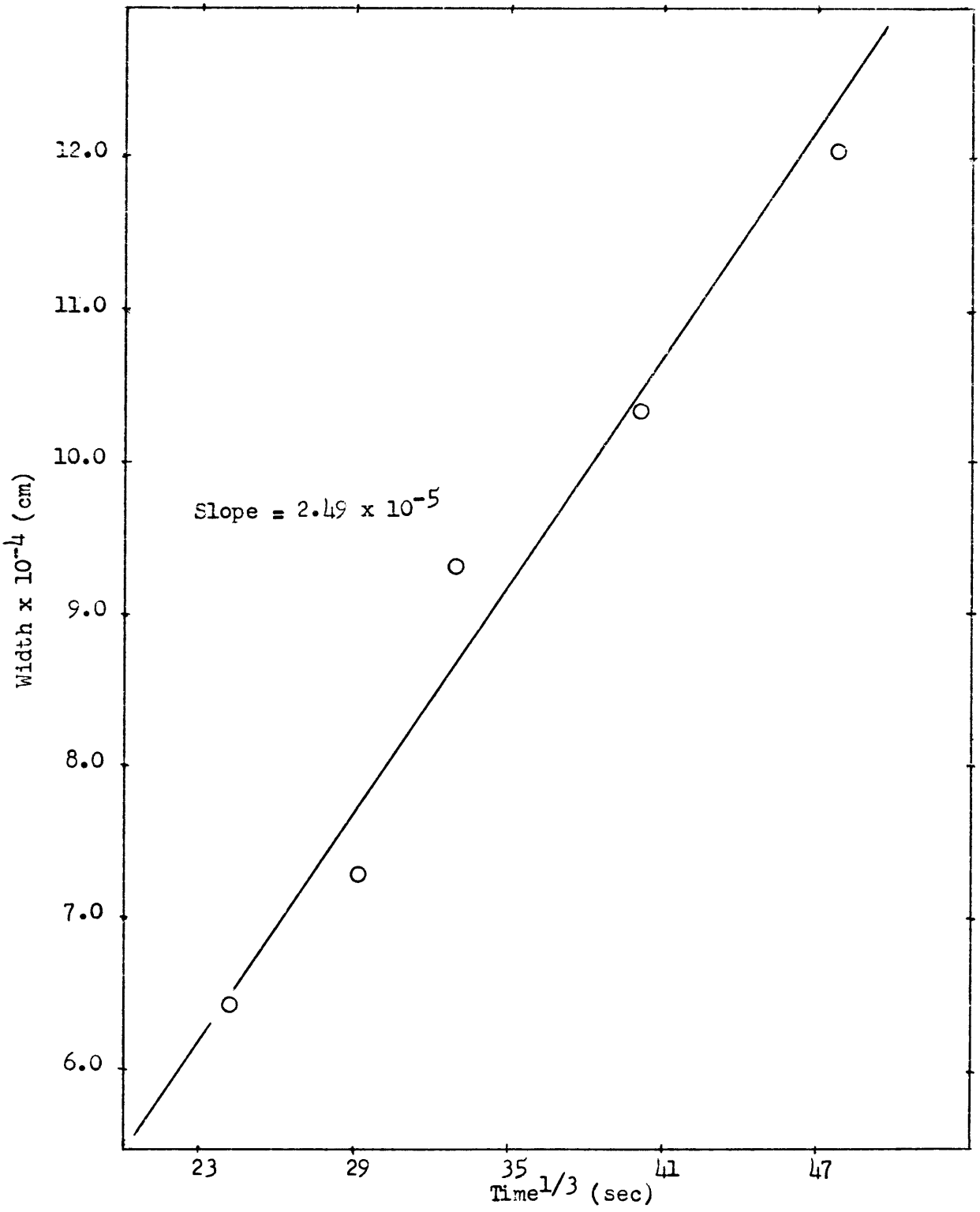

Figure 17. Graph of Groove Width vs. Time$^{1/3}$ for pure iron in liquid lithium at 700 C.

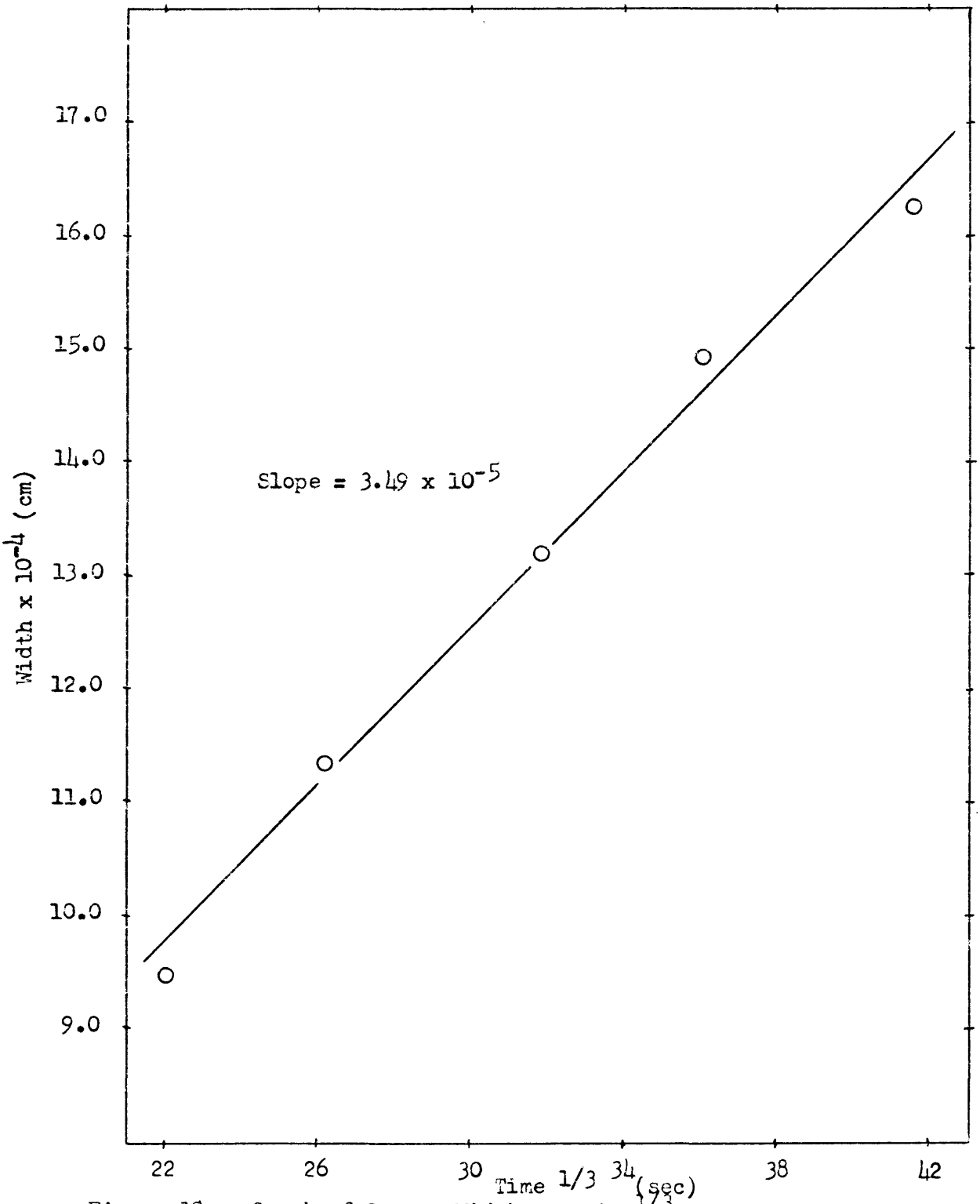

Figure 18. Graph of Groove Width vs. Time$^{1/3}$ for pure iron in liquid lithium at 750 C.

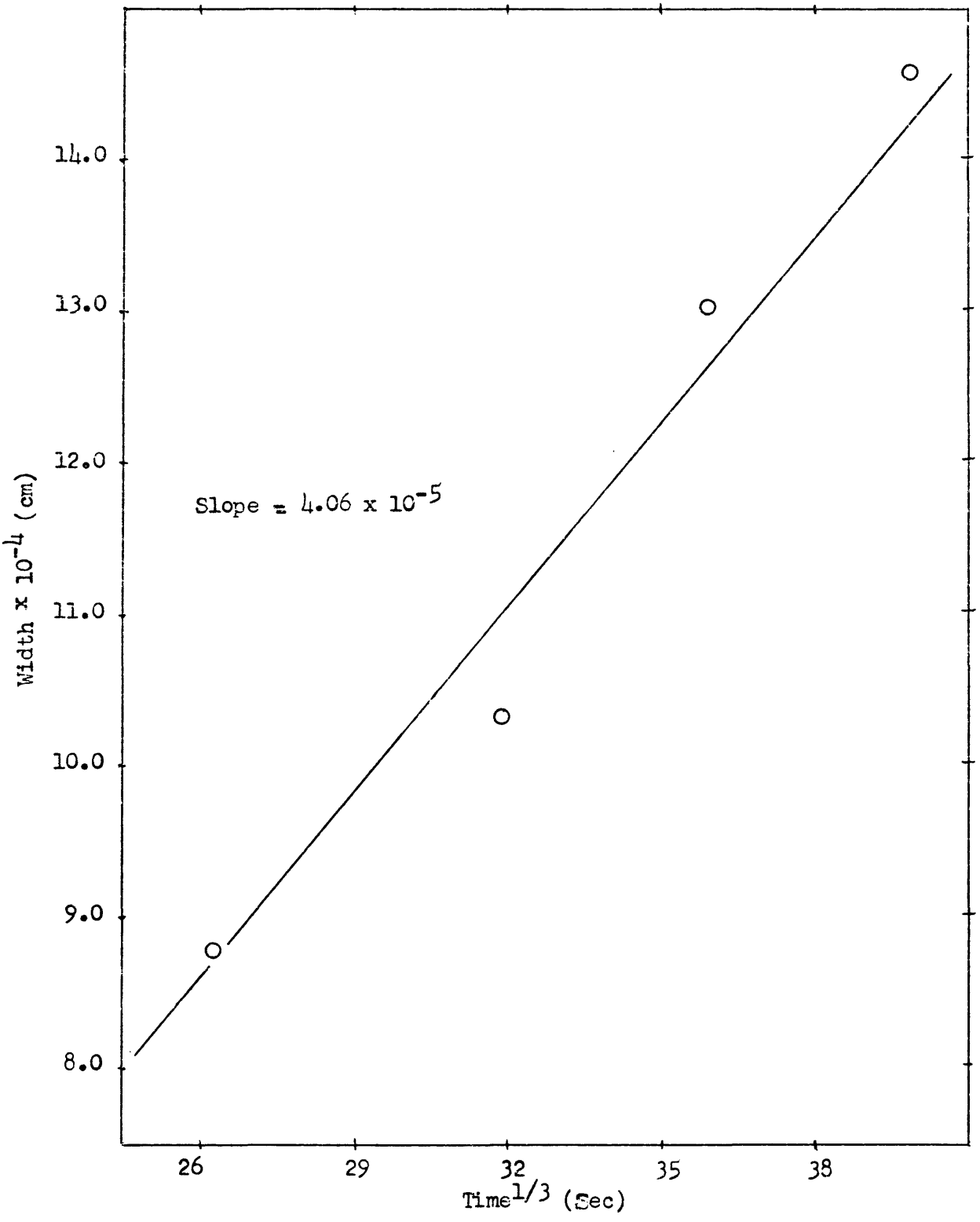

Figure 19. Graph of Groove Width vs. Time$^{1/3}$ for pure iron in liquid lithium at 500 C.

TABLE III

Rate coefficients obtained from the slope of the plots of width versus time$^{1/3}$

Temperature, ^{o}K	Rate Coefficients, K cm/sec$^{1/3}$
873	1.47×10^{-5}
923	1.83×10^{-5}
973	2.49×10^{-5}
1023	3.49×10^{-5}
1073	4.06×10^{-5}

The expression for the volume diffusion coefficient can be related to the measured rate coefficient by substitution of equation 17 into equation 21. The volume diffusion coefficient, D_V, is the given by

$$D_V = \frac{R^3 kT}{125\, \gamma_{sl} C_o \Omega^2} \tag{22}$$

Two parameters in equation 22 must be determined before the volume diffusion coefficient can be obtained. These are the interfacial tension, γ_{sl}, and the concentration of the diffusing atoms, C_o.

Two different techniques were used to obtain an approximate value for the interfacial tension. The first technique was based on Antonow's approximation[46] for the interfacial tension which is given by

$$\gamma_{sl} = \gamma_{sv} - \gamma_{lv} \tag{23}$$

where

γ_{sl} = interfacial tension between the solid and liquid phases

γ_{sv} = interfacial tension between the solid and vapor phases

γ_{lv} = interfacial tension between the liquid and vapor phases

The most recent measurement for the interfacial tension of alpha-iron, γ_{sv}, is reported to be 2320 ergs/cm^2[47]. Taylor[48] used the maximum bubble pressure method to measure the surface tension of lithium and found that at the melting point the surface tension was 398 ergs/cm^2 and the temperature coefficient to be -0.14 ergs/cm^2/°C. Thus at 700 °C,

the surface tension of lithium, γ_{lv}, would be 325 ergs/cm^2. Substitution of these values into equation 23 results in an interfacial tension between the solid alpha-iron and the liquid lithium to be approximately 2000 ergs/cm^2.

The other technique of obtaining the interfacial tension is from measurements of the dihedral angle of the thermal groove. Figure 20 illustrates the measurements required to determine this dihedral angle. The grain boundary root angle can not be measured directly from the photograph due to the nature of the interference microscopy. The magnification in the direction perpendicular to the fringes is much greater than in the direction parallel to the fringes, therefore, the "a" dimension is obtained by counting fringes and relating this to the half-wave length of the light source. A sodium light source was utilized thus the distance between fringes is 0.2945 cm. From this measured ϕ and knowledge of the grain boundary energy in iron, the interfacial tension can be obtained from the equilibrium expression

$$\gamma_{gb} = 2\,\gamma_{sl}\cos\phi \qquad (24)$$

Investigations on grain boundary energies by Inman and Tipler[49] reported a grain boundary energy, γ_{gb}, for pure iron to be 780 ergs/cm^2. The calculated value for the interfacial tension, γ_{sl}, was 2320 ergs/cm^2. This illustrates a reasonable agreement between the measured and calculated interfacial tension. For this investigation a value of 2000 ergs/cm^2 was chosen as the approximate value for this interfacial tension.

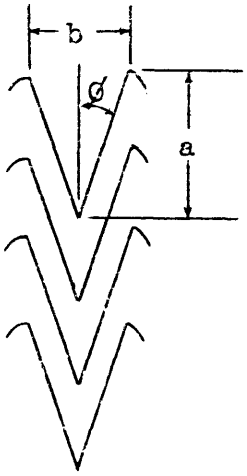

Figure 20. Illustration of the measurements required to determine the dihedral angle, ø.

The concentration of the diffusing atoms, C_o, will be dependent upon the path and temperature. In order to produce a thermal groove, iron must diffuse. There are four possible paths that must be considered (figure 21):

Case I Interfacial diffusion

Case II Volume diffusion through the solid alpha-iron

Case III Volume diffusion through the liquid lithium

Case IV Diffusion through a corrosion product

Interfacial diffusion, case I, can be eliminated as a possible path due to the results obtained and reported in Table II, which suggests the controlling process to be volume diffusion. For volume diffusion through the alpha-iron, case II, or through the corrosion product, case IV, the concentration of diffusing atoms can be treated as a constant and not a function of temperature. This assumes that the corrosion product has a definite stoichiometry, such as $Li_3N \cdot FeN$, which was suggested by Hoffman[10]. This corrosion product is expected to be a thin film on the solid-liquid interface.

If the diffusion path is occurring in the liquid lithium, the value of C_o will be dependent on the solubility of iron, and thus, upon temperature. Studies conducted by Leavenworth and Cleary[50] on solubilities on nickel, chromium, iron, titanium, and molybedenum in lithium at elevated temperatures are illustrated in figure 22. Thus, all the parameters in equation 22 have been defined and the diffusion coefficients can be obtained for two of the three paths, diffusion through the

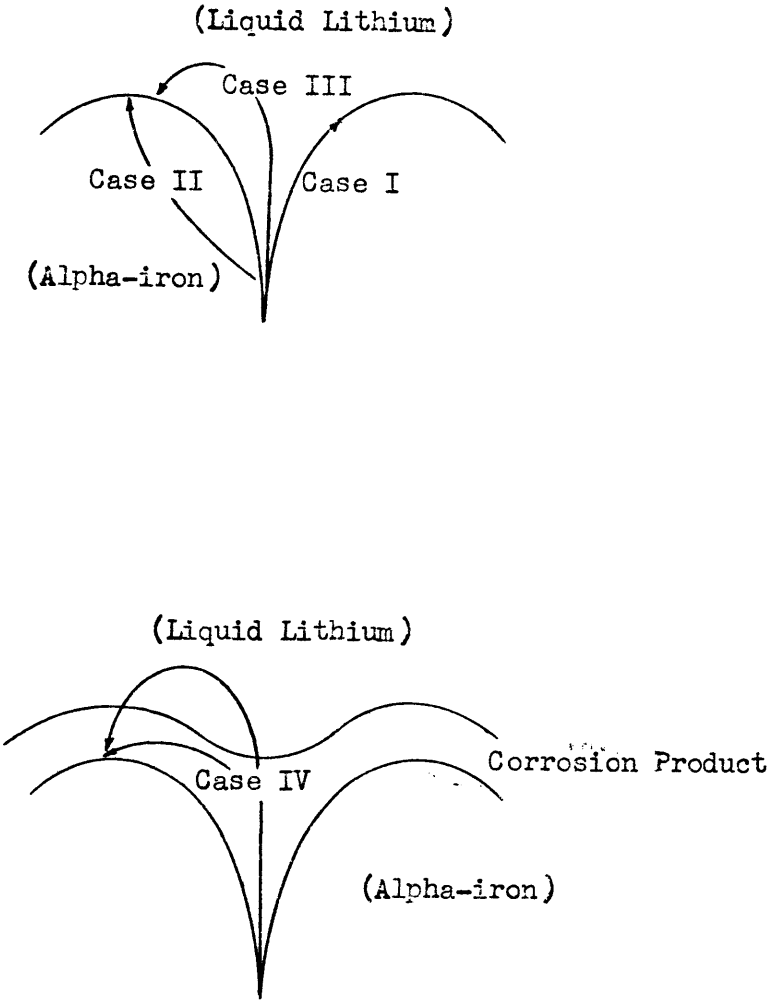

Figure 21. Illustration of the four possible paths for iron diffusion.

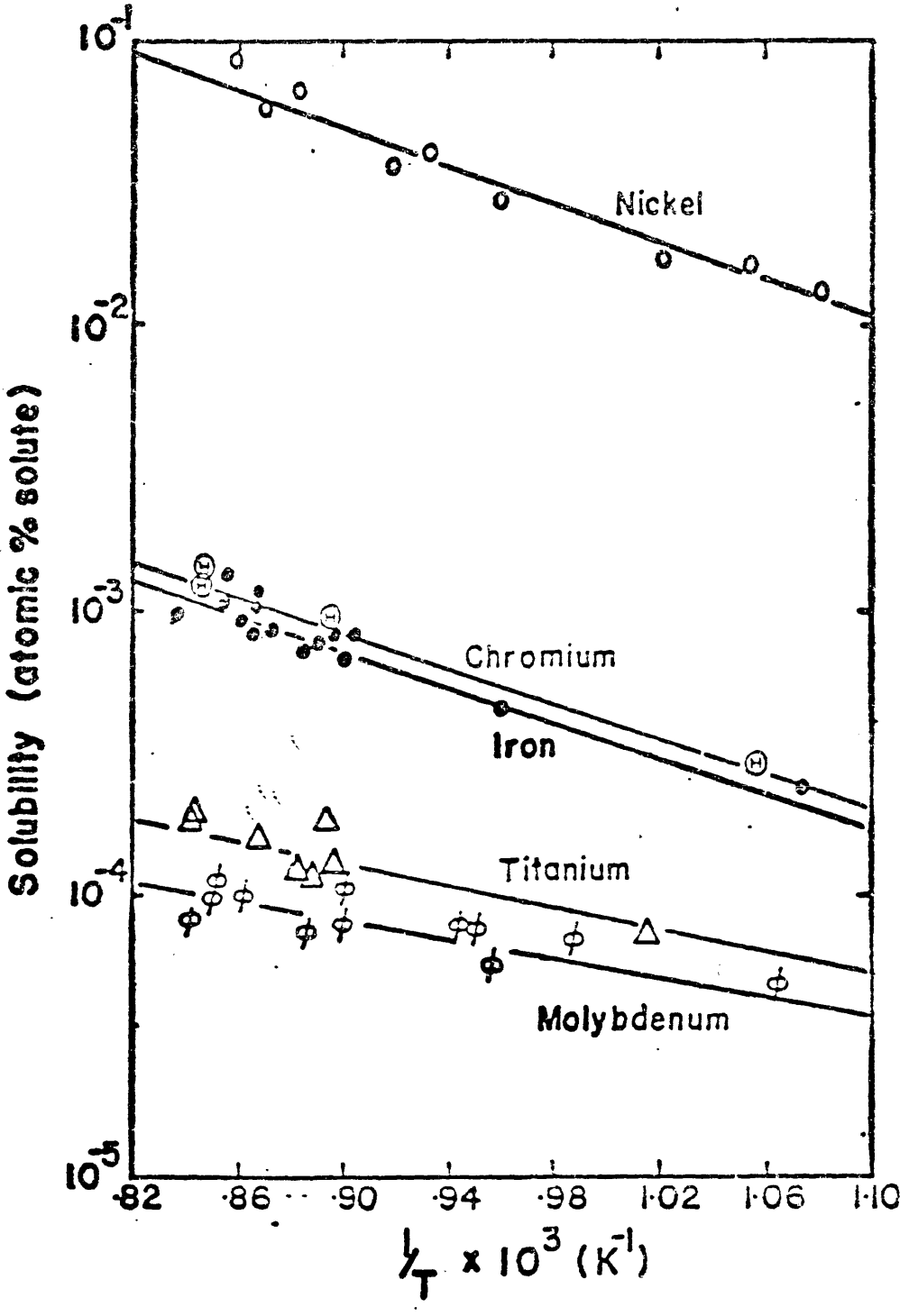

Figure 22 The temperature dependence of the solubilities of a number of metals.(50)

liquid lithium and diffusion through the alpha-iron. Table IV shows the resulting calculated diffusion coefficients for each path.

The Arrhenius plot for case II, where the diffusion path is assumed to be through the solid alpha-iron is shown in figure 23. The resulting activation energy obtained was approximately 31.9 Kcal./Mole which is not in agreement with the reported value of 57.3 Kcal./Mole[6] for self diffusion of iron in iron. In addition to this disagreement in activation energies, the diffusion coefficients in this investigation are of the magnitude of 10^{-10} to 10^{-12} cm^2/sec, whereas the diffusion coefficients for self diffusion in solids are expected to be of the magnitude of 10^{-12} to 10^{-14} cm^2/sec.[38,39] Thus on the basis of the value for the activation energy and the magnitudes of the diffusion coefficients, case II can be eliminated for the possible paths.

For case III, where the diffusion path is assumed to be through the liquid lithium, the Arrhenius plot is shown in figure 24. The apparent activation energy found was approximately 18 Kcal./Mole. Studies conducted in recent years on self diffusion in liquid metals,[51,55,56] have reported apparent activation energies less than 15 Kcal./Mole and diffusion coefficients of the magnitude of 10^{-4} cm^2/sec. Assuming the diffusion path is through the liquid lithium, the reported values for the activation energy and the magnitude of the diffusion coefficients are not consistent with the calculated values obtained from this investigation.

Swalin[52,53] considered liquid metal diffusion to be a cooperative process and not an activated process. He developed a statistical model

TABLE IV

Diffusion coefficients for diffusion through the alpha-iron and for diffusion through the liquid lithium.

Diffusion through the alpha-iron: (Case II)

Temperature ^{o}K	Diffusion coefficient, D_v, cm^2/sec
873	4.97×10^{-12}
923	1.02×10^{-11}
973	2.68×10^{-11}
1023	7.81×10^{-11}
1073	1.28×10^{-10}

Diffusion through the liquid lithium: (Case III)

Temperature ^{o}K	Diffusion coefficient, D_v, cm^2/sec
873	6.45×10^{-7}
923	8.80×10^{-7}
973	1.54×10^{-6}
1023	3.17×10^{-6}
1073	3.78×10^{-6}

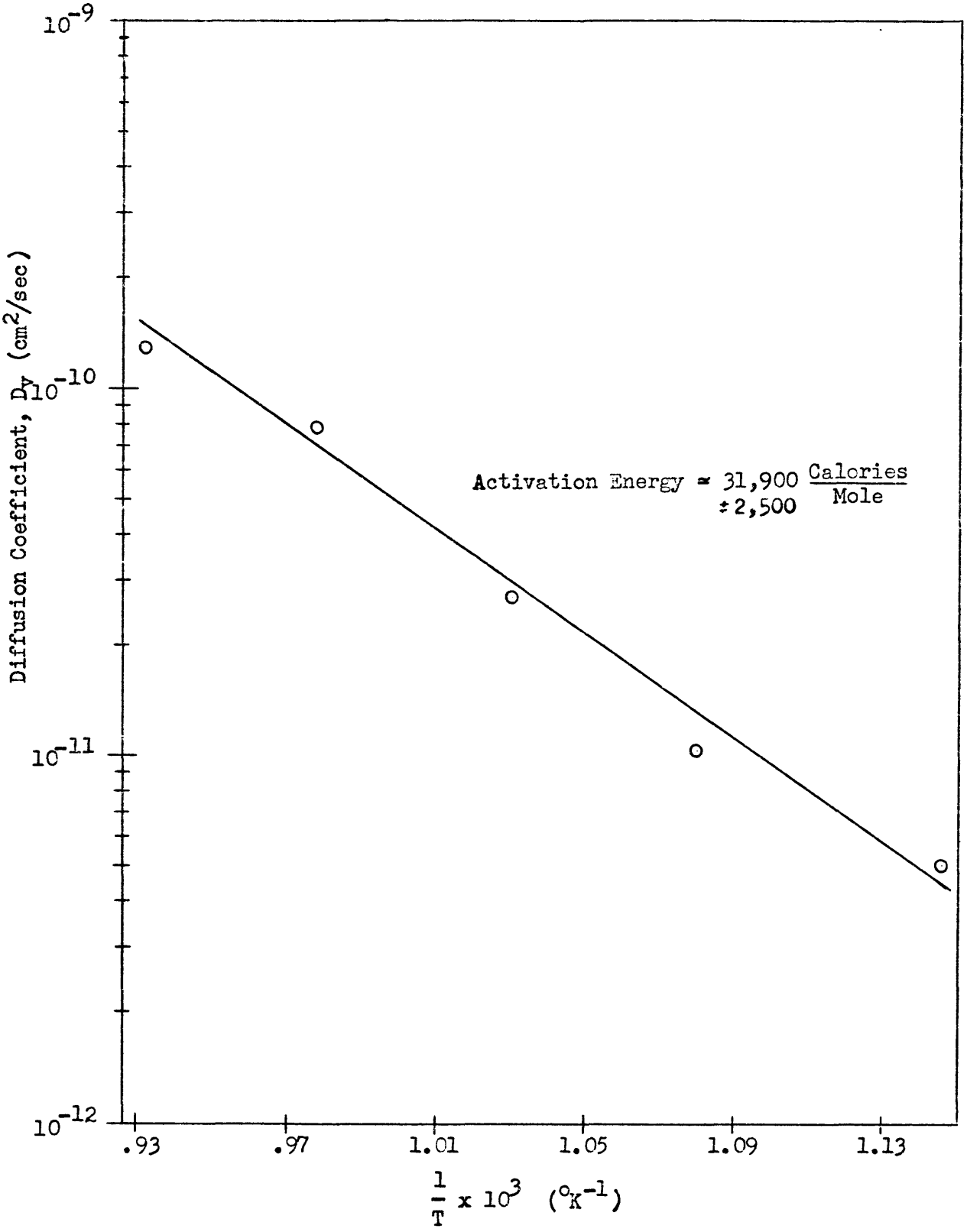

Figure 23. An Arrhenius plot for the case where the diffusion path is through the solid alpha-iron in an iron-liquid lithium system. C_C is known.

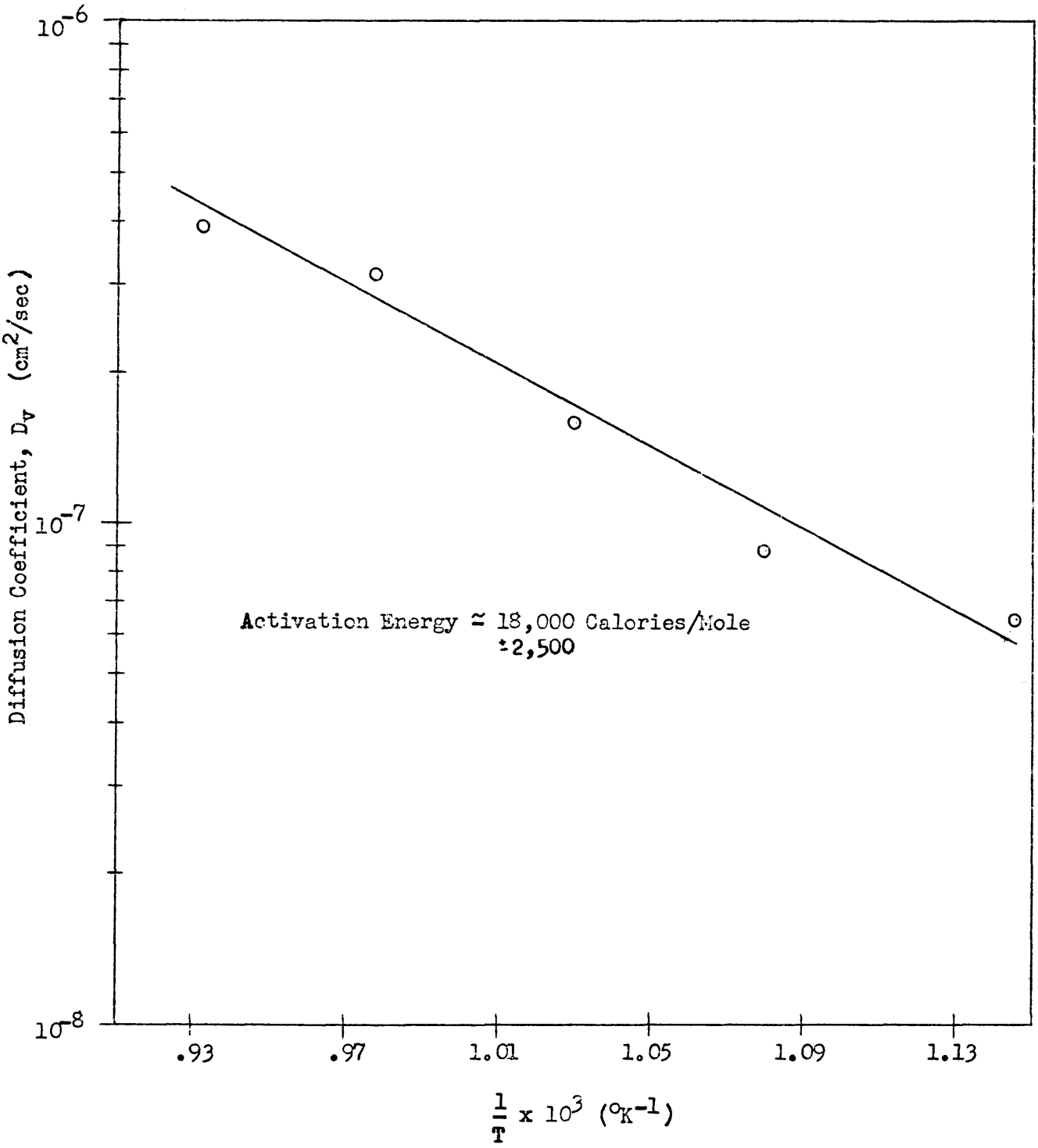

Figure 24. An arrhenius plot for the case where the diffusion path is through the liquid lithium in an iron-liquid lithium system. C_o is known

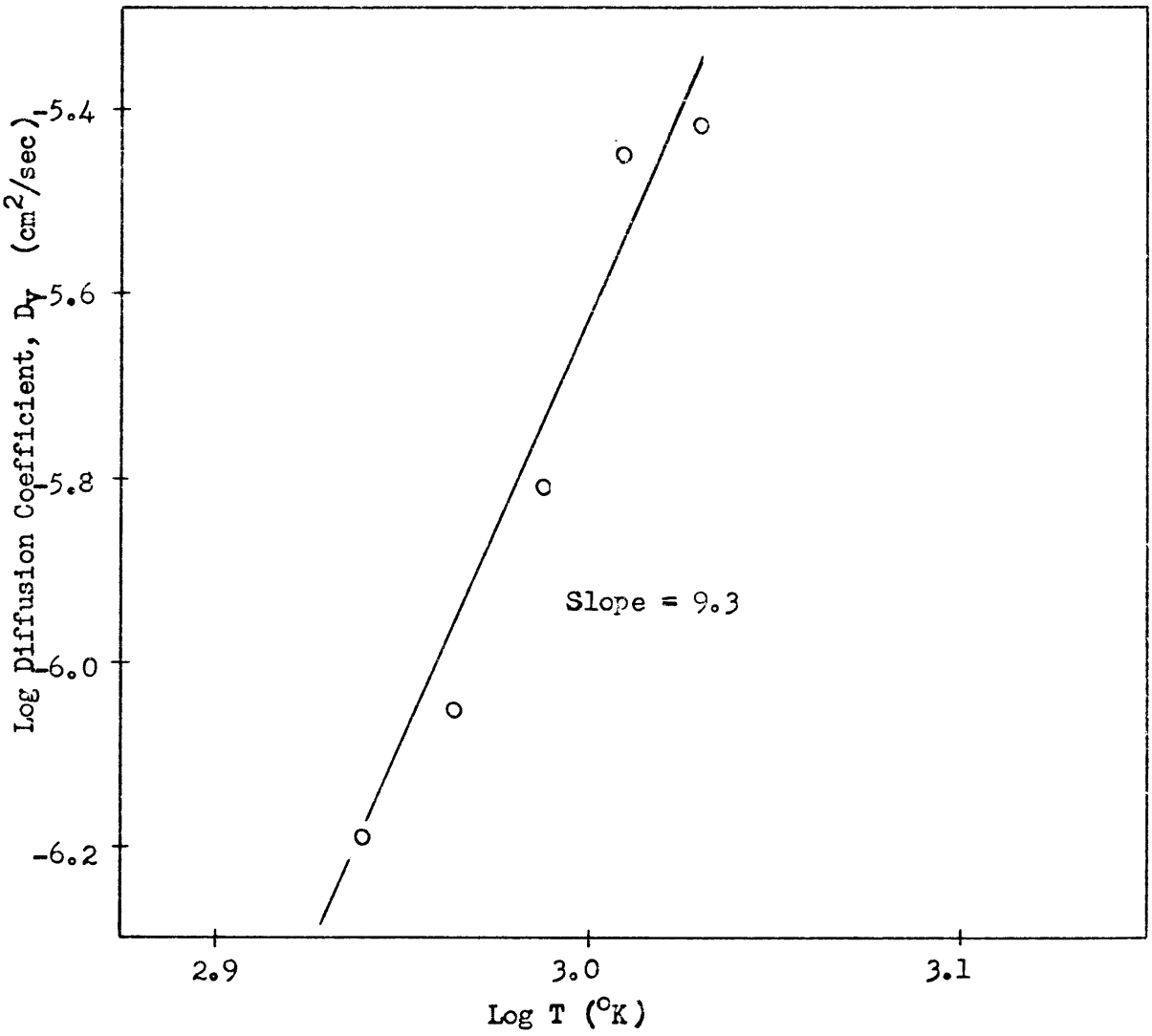

Figure 25. A plot of log D_V versus log T to obtain the temperature dependency of the diffusion coefficent, D_V.

for atom movement in liquid metals and found that the diffusion coefficient, D_v, to have T^2 dependency. Figure 25 illustrates that the results of this investigation are also not consistent with Swalin's liquid diffusion concepts. Thus on the basis of the value for the activation energy, the magnitudes of the diffusion coefficients, and disagreement with Swalin's theory, case III can be eliminated from the possible paths.

This investigation strongly suggests, by the process of elimination of the possible paths being considered, that there must exist a corrosion product film and that the rate controlling process is associated with volume diffusion in this corrosion product. The presence of this corrosion product could also explain the hindrance of the expected rate controlling process of interfacial diffusion as was reported for the similar iron-liquid sodium system.(44)

For thermal grooving of pure iron in nitrogen saturated liquid lithium there are three major diffusing species. These are iron, lithium, and nitrogen. The value of the concentration of diffusing atoms, C_o, is unknown. However, by assuming that the corrosion product has a definite stoichiometry, C_o can be treated as a constant. With the measured rate coefficients, K, established, log K^3T versus 1/T was plotted as illustrated in figure 26. The resulting activation energy was found to be 32 Kcal./Mole.

Previous investigations done by Patterson(12) and Reeves(13) have reported approximately the same activation energies of 31.1 Kcal./Mole for the grain boundary penetration of 304L and nitrided 304L stainless

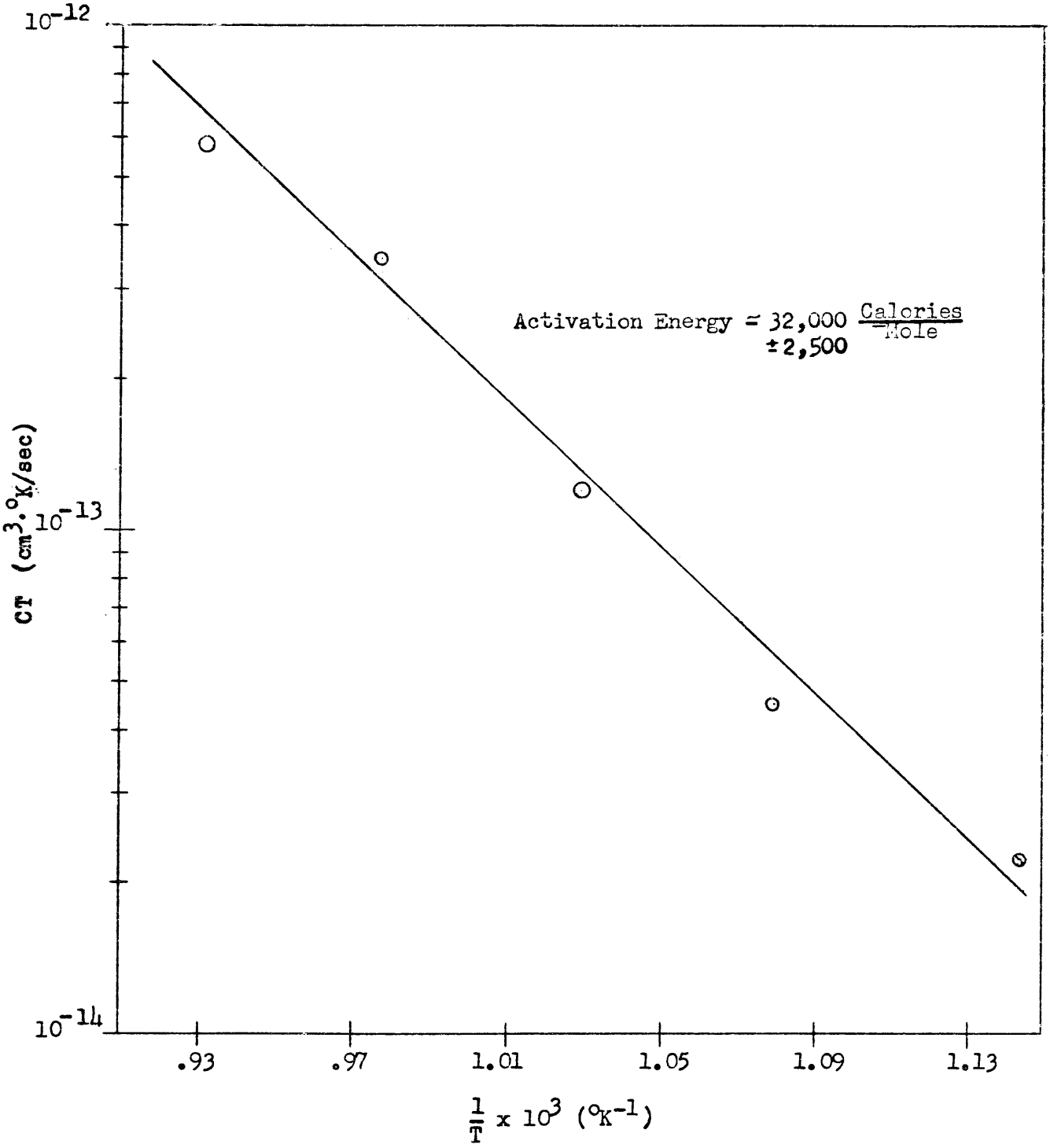

Figure 26. An Arrhenius plot for the case where the diffusion path is through a corrosion product in an iron-liquid lithium system. C_o is a constant.

steel by liquid lithium. From their investigations the rate controlling mechanism was found to be the lithium diffusion in the grain boundary corrosion product. Nitrogen was found to influence the rate of penetration, but not to effect the controlling mechanism.

This agreement between the activation energy for the diffusion in the grain boundary corrosion product and the activation energy for this investigation suggests that the rate controlling mechanism is the lithium diffusion in this corrosion product film.

Since the corrosion product has been suggested[10] to be a covalent compound of the form $Li_3N \cdot FeN$, the mass transport of iron in this corrosion product is a coupled diffusion phenomena. There are continually three diffusing species (Li, N, and Fe ions) migrating in this corrosion product governed by their vacancy concentrations, their jump frequencies, and overall charge neutrality. The slowest diffusing specie will control the overall mass transport behavior. This is similar to the model described by Feingold et al[43] for the grain boundary grooving kinetics for a nickel - Al_2O_3 interface where it was also necessary to consider coupled diffusion and charge neutrality.

The coupled diffusion coefficient for the mass transport in a general compound, A_aB_b, has been given by Feingold et al[43] to be of the form:

$$D_c = \frac{D_A D_B}{aD_B + bD_A} \tag{25}$$

where

D_c = coupled diffusion

D_A = diffusion coefficient for specie A

D_B = diffusion coefficient for specie B

If $D_B >> D_A$, in the case where A is the slowest diffusing specie, then equation 25 reduces to

$$D_c = \frac{D_A}{a} \tag{26}$$

and the activation energy for D_c becomes that for D_A, the slowest specie.

This investigation has determined the nature of the mass transport phenomena occurring at, or near, the liquid lithium-solid interface and has related this behavior to the kinetics involved in lithium penetration of ferrous alloy grain boundaries. A coupled diffusion model has been proposed to explain the mass transport through the corrosion product which has been suggested to be at the grain boundaries and the liquid-solid interface. The lithium ion diffusion jump was proposed to be the rate controlling process for the coupled diffusion. This investigation has demonstrated the utility of using grain boundary grooving analysis to gain a further understanding of the complex corrosion phenomena occurring in the containment of liquid lithium by ferrous alloys.

CONCLUSIONS

The most important facts this investigation revealed are:

(1) The principal mechanism for grain boundary grooving of pure iron in nitrogen saturated liquid lithium is volume diffusion.

(2) The apparent activation energy for grain boundary grooving of pure iron in the corrosion product is approximately 31.9 Kcal/Mole.

(3) By deduction of possible volume diffusion paths and activation energy agreement with previous grain boundary penetration results, findings suggest that the controlling activated step for the mass transport of iron is the diffusion jump of lithium in the corrosion product.

(4) The alpha iron-liquid lithium interfacial energy can be approximated to be 2000 ergs/cm^2.

SUGGESTIONS FOR FURTHER RESEARCH

The results of this investigation suggest areas for further research:

(1) An investigation to isolate and identify the corrosion product and its physical properties

(2) The need for a method to accurately measure and control oxygen and nitrogen impurities in lithium.

APPENDIX I

Outline for Herring's derivation of the expression given by:

$$\mu = \mu_0 + \Omega \left(\gamma + \frac{\partial^2 \gamma}{\partial n_x^2} \right) K$$

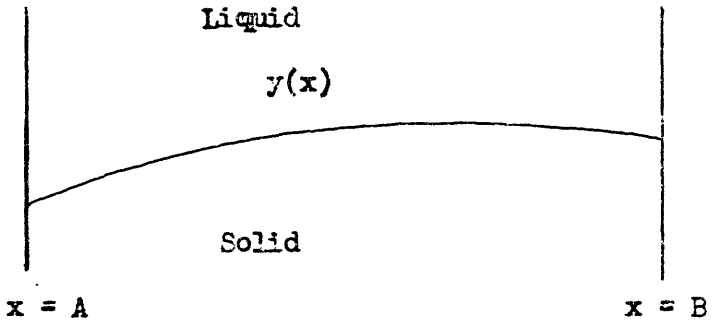

Arc length = s

The specific surface free energy, f_s, is given by

$$f_s = \gamma + \sum_{i=1}^{n} \mu_i \Gamma_i \tag{1a}$$

Considering a single component system, $\Sigma \mu_i \Gamma_i = 0$, the specific surface free energy is given by

$$f_s = \gamma = F \tag{2a}$$

Integrating γ along the surface, y(x), from A to B gives the total surface free energy per unit depth.

$$F = \int_A^B \gamma \, ds \tag{3a}$$

The incremental distance along a curve, ds, is given by

$$ds = \dot{y}(1 + \dot{y}^2)^{1/2}dx \tag{4a}$$

let

$$G(\dot{y}) = \gamma \dot{y}(1 + \dot{y}^2)^{1/2} \tag{5a}$$

therefore

$$F = \int_A^B G(\dot{y})dx \tag{6a}$$

Now consider an infinitesimal rearrangement of material that gives a new surface defined by

$$y'(x) = y(x) + \delta y(x) \tag{7a}$$

Assuming end points remain stationary

$$\delta y(A) = \delta y(B) \tag{8a}$$

and

$$\int_A^B \delta y(x) = 0 \tag{9a}$$

The variation in F is given by the standard procedure used in calculus of variations.

$$\delta F = \int_A^B \frac{dG}{d\dot{y}} \delta \dot{y}dx \tag{10a}$$

and

$$\delta F = \int_A^B \frac{dG}{d\dot{y}} \delta y dx = \int_A^B \frac{dG}{d\dot{y}} \frac{d}{dx}(\delta y)dx \tag{11a}$$

where

$$\delta \dot{y} = \frac{d(\delta y)}{dx} \tag{12a}$$

If the end points remain stationary then δy at A and B vanishing and partial integration of equation 11a results in

$$\delta F = -\int_A^B \frac{d}{dx}\left(\frac{dG}{d\dot{y}}\right)\delta y dx \tag{13a}$$

Now assume $\mu' = \mu - \mu_o$, where μ' equals the chemical potential for the new surface and μ_o is a constant, is uniquely defined for all points on the surface y(x). The change in the specific surface free energy, δF, is also given by

$$\delta F = \frac{1}{\Omega}\int_A^B (\mu - \mu_o)\,\delta y ds \tag{14a}$$

and $(\delta y dx)/\Omega$ determines the number of atoms added to the interval dx, therefore

$$\delta F = \frac{1}{\Omega}\int_A^B \mu\,\delta y dx \tag{15a}$$

Subtracting equation 13a form equation 15a results in

$$0 = \int_A^B \left[\frac{d}{dx}\left(\frac{dG}{d\dot{y}}\right) + \frac{\mu}{\Omega}\right]\delta y dx \tag{16a}$$

However δy is arbitrary so that the arguement within the brackets must equal zero, therefore

$$\mu = -\Omega\frac{d}{dx}\left(\frac{dG}{d\dot{y}}\right) \tag{17a}$$

Substitution of equation 5a into equation 17a gives

$$\mu = -\Omega\frac{d}{dx}\left(\frac{d}{dy}\left[\gamma\dot{y}(1+\dot{y}^2)^{1/2}\right]\right) \tag{18a}$$

and using the idenities

$$\frac{d\gamma}{dy} = \frac{1}{1+\dot{y}^2}\frac{d\gamma}{d\theta} \tag{19a}$$

where

$$\theta = \tan^{-1}\dot{y} \tag{20a}$$

and

$$\frac{d}{dx} = \dot{y}\frac{d}{d\dot{y}} \tag{21a}$$

Using equation 19a and equation 21a, the differentiation of equation 18a results in the expression

$$\mu = -\Omega(\gamma + \gamma'')\frac{\dot{y}}{(1+\dot{y}^2)^{3/2}} \tag{22a}$$

where for a curved surface concave toward the solid, K is given by

$$K = -\frac{\ddot{y}}{(1+\dot{y}^2)^{3/2}} \tag{23a}$$

therefore

$$\mu = \Omega(\gamma - \gamma'')K \tag{24a}$$

APPENDIX II

Outline for Mullins' derivation for grain boundary grooving by volume diffusion.

Assumptions:

1. The interfacial surface tension is independent of crystal orientation.
2. The Gibbs-Thompson relation between curvature and chemical potential is assumed to determine the concentration of S atoms at the solid-solvent interface.
3. Convection is to be negligible in the fluid phase.

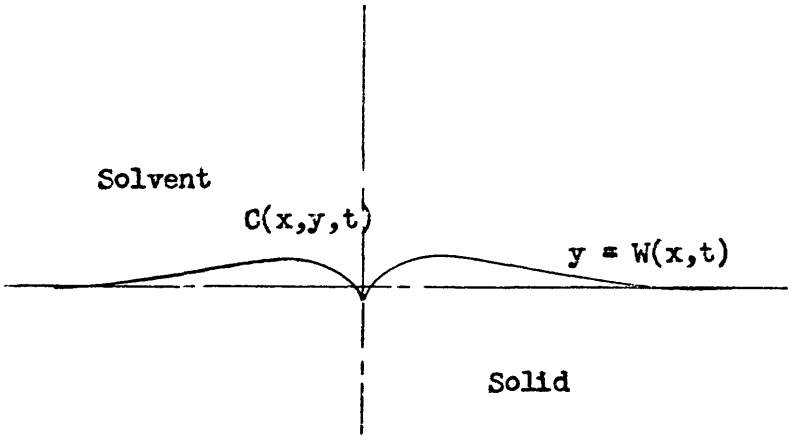

Figure 1b. Profile of a thermal groove.

Boundary conditions for W:

$$(\partial W/\partial x)_{x=0} = m \qquad (1b)$$

and

$$W(x,0) = 0 \tag{2b}$$

Let K denote curvature so that

$$K(x,t) = -\partial^2 W/\partial x^2 \tag{3b}$$

and let $C(x,y,t)$ be the concentration of solute in the solvent. The development of the interface may be stated as follows: For any given profile, $y = W(x,t_o)$, at time t_o, there will be a steady-state concentration field $C(x,y,t_o)$ which must satisfy Laplace's equation in the solvent and must reduce to given values (proportional to $K(x,t)$) on the interface. From this concentration field the value of $(\partial C/\partial y)_{y=0}$ and hence the normal flux of S atoms is determined for all elements of the interface. But the normal flux determines the rate of movement the interface $\partial W/\partial t$ and hence the new profile $y = W(x,t_o+\Delta t)$ at time $t_o+\Delta t$. The objective is to formulate an equation for $W(x,t)$, from which the diffusion problem has been eliminated, and then to solve it under conditions given by equations 1b and 2b.

First we require $C(x,y,t)$ to satisfy the equations:

$$\nabla^2 C = 0 \tag{4b}$$

$$C(x,0,t) = C_o + C_o \frac{\gamma_{sl}\Omega}{kT} K(x,t) \tag{5b}$$

Equation 5b is the Gibbs-Thompson relation. The solution of equation

4b that satisfies equation 5b is

$$C(x,y,t) = C_o + C_o \frac{\gamma_{sl}\Omega}{kT}\frac{2}{\pi}\int_0^\infty d\omega \cos(\omega x)e^{-\omega y}\int_0^\infty K(\epsilon,t)\cos\omega\epsilon\, d\epsilon \quad (6b)$$

Equation 6b satisfies equation 4b may be verified by substitution and that equation 6b satisfies equation 5b follows from the fact that for y = 0, the double integral is simply the fourier integral for K(x,t).

The rate of motion of an element of surface is given by

$$\partial W/\partial t = D\Omega(\partial C/\partial y)_{y=0} \quad (7b)$$

where D is the diffusion coefficient of S atoms in the solvent. Differentiating equation 7b twice with respect to x to express the relation in terms of curvature gives

$$\frac{\partial K}{\partial t} = -D\Omega\frac{\partial^2}{\partial x^2}\left[\left(\frac{\partial C}{\partial y}\right)_{y=0}\right] \quad (8b)$$

Substitution of equation 6b into equation 8b results in

$$\frac{\partial K}{\partial t} = A'\frac{2}{\pi}\int_0^\infty d\omega\,\omega^2\cos\omega x\int_0^\infty K(\epsilon,t)\cos\omega\epsilon\, d\epsilon \quad (9b)$$

where

$$A' = \frac{C_o\gamma D\Omega^2}{kT} \quad (A' = C \text{ in the text})$$

Integrating equation 9b twice using equations 1b and 2b to obtain the

the profile $y = W(x,t)$, the results are

$$y = W(x,t) = m(A't)^{1/3} \chi\left[\frac{x}{(A't)^{1/3}}\right] \qquad (10b)$$

where the function $\chi(u)$ is calculated from a power series and plotted below.

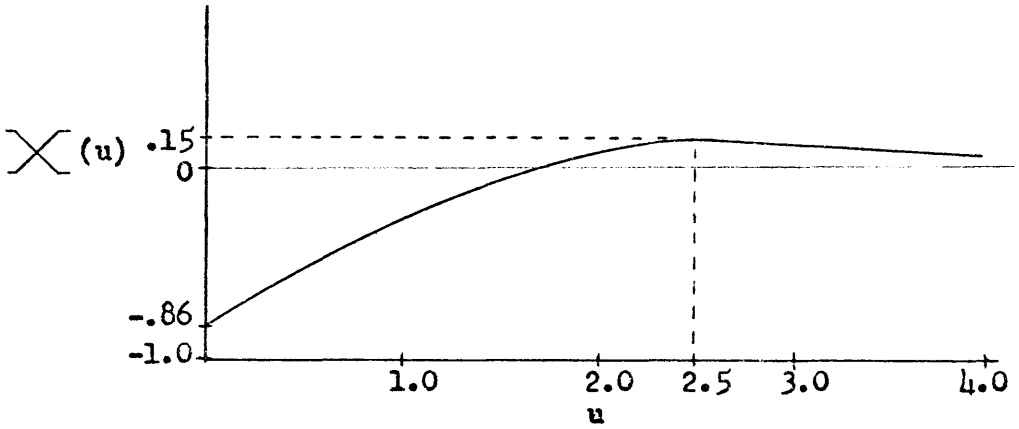

Figure 2b. Normalized profile shape due to volume diffusion.

It follows from equation 10b and the information in figure 2b that the depth of the groove, d, is

$$d_v = 1.01\ m(A't)^{1/3}$$

and the width of the groove, w, is

$$w_v = 5.0\ (A't)^{1/3}$$

APPENDIX III

Experimental Data

Grain Boundary Grooving Data:

	Time (sec) x 10^4	Width (cm) x 10^{-4}
600°C	6.84	7.54
	10.44	8.48
	15.84	9.66
	22.32	10.51
650°C	2.88	5.34
	4.68	6.44
	7.20	7.46
	10.80	8.31
	16.20	9.83
700°C	1.44	6.44
	2.52	7.29
	3.60	9.32
	6.48	10.34
	10.44	12.03
750°C	1.08	9.49
	1.80	11.36
	3.24	13.22
	4.68	14.92
	7.20	16.27
800°C	1.80	8.81
	3.24	10.34
	5.04	13.05
	6.84	14.58

REFERENCES

1. S. A. Jansson (ed.), Chemical Aspects of Corrosion and Mass Transfer in Liquid Sodium, AIME (1971).

2. J. E. Draley and J. R. Weeks (eds.), Corrosion by Liquid Metals, Plenum Press, New York (1970).

3. E. E. Hoffman and W. D. Manly, Symposium on Handling and Uses of Alkali Metals, American Chem Soc., 82 (1957).

4. W. F. Brehm Jr. and C. Y. Li, Trans. AIME, 242, 1205 (1968).

5. R. L. Klueh, Corrosion by Liquid Metals, Plenum Press, New York, 177 (1970).

6. D. Graham and D. Tomlin, Phil. Mag., 8, 1581 (1963).

7. A. J. Romano, C. J. Klamut and J. R. Weeks, Chemical Aspects of Corrosion and Mass Transfer in Liquid Sodium, AIME, 223 (1971).

8. R. N. Lyon, Liquid Metals Handbook 2nd Edition. USAEC and Department of the Navy, Report NAVEXOS, 73 (1952).

9. J. R. DiStefano and E. E. Hoffman, Corrosion of Reactor Materials, 2, (1962).

10. E. E. Hoffman, Corrosion of Metals by Lithium at Elevated Temperatures, CRNL 2924.

11. A. S. Brasunas, Liquid Metal Corrosion, 9, 78 (1953).

12. R. A. Patterson, Liquid Lithium Corrosion of 304L Stainless Steel, M. S. Thesis, Colorado School of Mines, T-1684 (1974).

13. J. A. Reeves, Liquid Lithium Corrosion of Nitrided 304L Stainless Steel, M. S. Thesis, Colorado School of Mines, T-1703 (1974)

14. W. W. Mullins, J. Appl. Phys., 28, 335 (1957).

15. P. Roy, D. Dutina and F. Comprelli, Liquid Metal Corrosion, Plenum Press, New York, 1 (1970).

16. J. R. Weeks and H. S. Isaacs, Advances in Corrosion Science and Technology, Plenum Press, New York, 3, (1973).

17. R. B. Snyder, Journal of Nuclear Materials, 259 (1974).

18. E. E. Hoffman, Corrosion Fundamentals, University of Tennessee Press, 78 (1956).

19. V. I. Nikitin, Fizikic-Khimicheskaya Mekhanika Materialov, 4, No. 1, 13 (1968).

20. W. W. Mullins, Metal Surfaces, ASM, Metals Park, 17 (1962).

21. W. E. Kingston (ed), The Physics of Powder Metallurgy, McGraw Hill, New York, (1951).

22. C. R. Austin and B. S. Norris, Trans. AIME, 131, 349 (1938).

23. C. Herring, Physics of Powder Metallurgy edited by Kingston, Mcgraw Hill, New York (1951).

24. J. K. Mackenzie, A. J. W. Moore and J. F. Nichols, J. Phys. Chem. Solids, 23, 185 (1962).

25. H. Mykura, Acta Met., 9, 570 (1961).

26. W. L. Winterbottom and N. A. Gjostein, Acta Met., 14, 1041 (1966).

27. P. G. Shewmon and W. M. Robertson, Metal Surfaces, Structure, Energetics and Kinetics, ASM, 67 (1963).

28. P. G. Shewmon, Diffusion in Solids, McGraw Hill Book Co., New York, (1963).

29. W. W. Mullins, J. Appl. Phys., 30, 77 (1959).

30. R. T. King and W. W. Mullins, Acta Met., 10, 601 (1962).

31. W. W. Mullins, Trans. AIME, 218, 354 (1960).

32. F. A. Nichols and W. W. Mullins, Trans AIME, 233, 1840 (1965).

33. J. M. Blakely, Progr. in Mat. Sci., 10, 395 (1963).

34. N. A. Gjostein, Metal Surfaces, Structure, Energetics and Kinetics, ASM, (1963).

35. F. J. Bradshaw and R. H. Brandon, Royal Aircraft Extablishment, Technical Note No. CFM76 (1964).

36. J. M. Blakely, Trans. Faraday Soc., 57, 1164 (1961).

37. N. A. Gjostein, Trans AIME, 239, 785 (1967).

38. N. A. Gjostein, Trans AIME, 221, 1039 (1961).

39. J. Y. Choi and P. G. Shewmon, Trans AIME, 224, 589 (1962).

40. D. L. Olson, H. R. Patil and J. B. Blakely, Scripta Met., 6, 229 (1972).

41. J. Kruger and K. H. Stern, J. Electrochem. Soc., 109, 889 (1962).

42. C. A. Steidel, Che-Yu Li and C. W. Spencer, Trans AIME, 230, 84 (1964).

43. A. H. Feingold, Solid-State Reactions at the Nickel-Aluminum Oxide Interface, PhD Thesis, Cornell University, #681 (1967).

44. J. G. Eberhart, F. A. Cafasso, H. M. Feder and W. Kremsner, Corrosion by Liquid Metals edited by J. D. Draley and J. R. Weeks, Plenum Press, New York, 461 (1970).

45. B. C. Allen, Trans Met. Soc. AIME, 236, 915 (1966).

46. G. Antonow, J. Chim. Phys., 5, 372 (1907).

47. E. D. Hondros, Acta Met., 16, 1377 (1968).

48. J. W. Taylor, Phil. Mag., 46, 867 (1955).

49. M. C. Inman and H. R. Tipler, Met. Review, 8, 105 (1963).

50. H. W. Leavenworth and R. L. Cleary, Acta Met., 9, 519 (1961).

51. L. Yang, M. T. Simnad and G. Derge, Trans Met. Soc. AIME, 206, 1577 (1956).

52. R. A. Swalin, Acta Met., 7, 736 (1959).

53. R. A. Swalin, Z. Naturforsch, 23a, 805 (1968).

54. H. A. Walls, Techniques in Metals Research, 4 (1968)

55. T. Ejima, Impurity Diffusion in Liquid Metals, Dept. of Met., Tohoku Univ.,Sendal, Japan (1972)